Formation of nanoscale spatially indirect excitons: Evolution of the type-II optical character of CdTe/CdSe heteronanocrystals

Celso de Mello Donegá*
Condensed Matter and Interfaces, Debye Institute for Nanomaterials Science, Utrecht University, Princetonplein 5, 3508 TA Utrecht, The Netherlands
(Received 20 July 2009; revised manuscript received 24 November 2009; published 1 April 2010)

In this work, the evolution of the optical properties of nanoscale spatially indirect excitons as a function of the size, shape, and composition of the heteronanostructure is investigated, using colloidal CdTe/CdSe heteronanocrystals (2.6 nm diameter CdTe core and increasing CdSe volume fraction) as a model system. Emphasis is given to quantitative aspects such as the absorption cross section of the lowest-energy exciton transition (μ_{SS}), Stokes shift, linewidths, and the exciton radiative lifetime. The hole wave function remains confined to the CdTe core while the electron wave function is initially delocalized over the whole heteronanocrystal (*type-I*$^{1/2}$ *regime*), and gradually localizes in the CdSe segment as the growth proceeds, until the spatially indirect exciton transition becomes the lowest-energy transition (*type-II regime*). This results in a progressive shift of the optical transitions to lower energies, accompanied by a decrease in the oscillator strengths at emission energies and an increase in the exciton radiative lifetimes. The onset of the type-II regime is characterized by the loss of structure of the lowest-energy absorption band, accompanied by a simultaneous increase in the Stokes shift values and transition linewidths. This can be understood by considering the dispersion of the hole and electron states in k space. The μ_{SS} values decrease rapidly in the type-I$^{1/2}$ regime but only slightly in the type-II regime. This shows that the indirect exciton formation leads primarily to redistribution of the oscillator strength of the lowest-energy transition over a wider frequency range. The total absorption cross section *per* ion-pair unit (i.e., integrated over all the exciton transitions) remains essentially constant during the heteronanocrystal growth, demonstrating that μ_{SS} is redistributed from higher-energy transitions of both the CdTe and the CdSe segments, in response to the reduction in the electron-hole wave-function overlap. Two radiative decay rates are observed and ascribed to exciton states with different degrees of localization of the electron wave function (an upper state with a faster decay rate and a lower state with a slower decay rate). The results presented here provide fundamental insights into nanoscale spatially indirect exciton transitions, highlighting the crucial role of a number of parameters (viz., electron-hole spatial correlation, exciton dispersion and exciton degeneracy, shape effects, and electronic coupling).

DOI: 10.1103/PhysRevB.81.165303 PACS number(s): 78.67.Bf, 73.22.−f, 71.35.Cc, 78.55.Et

I. INTRODUCTION

Semiconductor heterostructures have been extensively investigated and explored over the last decades, and are currently used in technological applications such as photovoltaic and optoelectronic devices. The band alignment between the materials that are combined in the heterostructure is of paramount importance, as it determines the localization regime of excited charge carriers (viz., type-I or type-II).[1] In type-I heterostructures, the band gap of one semiconductor lies entirely within the gap of the other material, and therefore after photoexcitation, both electron and hole will localize in the narrower band-gap semiconductor, resulting in a direct exciton. Conversely, type-II heterostructures possess a staggered band alignment, which leads to spatial separation of the electron and hole on different sides of the heterojunction, creating a spatially indirect exciton with properties that can be manipulated by choosing suitable combinations of materials.

Heteronanostructured materials offer additional degrees of control over the indirect exciton properties. In nanoscale systems with dimensions comparable to (or smaller than) the electron and hole Bohr radii, there is no true charge-carrier separation, which results in enhanced electron-hole (e-h) wave-function overlap, providing an additional tool to control the indirect exciton properties.[2] Since the position of the energy levels in quantum-confined semiconductor nanocrystals (NCs) is governed by size and dimensionality,[3] the relative energy offsets in semiconductor heteroNCs can be tuned by a judicious control of the composition, size, and shape of each component. This offers the possibility of directly controlling the electron-hole wave-function overlap and gives rise to an intermediate carrier localization regime in which one carrier is confined in one of the heteroNC components while the other is delocalized over both materials.[1,2,4] This flexibility in tailoring the optoelectronic properties of the heteronanostructure has important consequences for a number of technologies, and opens up interesting application possibilities: miniaturized low-threshold lasers,[2] photovoltaic devices,[5] fast optical switches,[6] systems for quantum information processing,[7] advanced IR detectors,[8] fast access memories,[9] spintronic devices,[10] and labels for biomedical imaging[11] and optical "nanoscopy" (i.e., super-resolution optical microscopy based on stimulated emission depletion[12]). The realization of this wide range of potential applications requires a strict control over the fabrication of the heteronanostructures and a thorough understanding of their properties. This has turned the investigation of type-II semiconductor heteronanostructures into a captivating research topic, which is attracting increasing attention worldwide.

Type-II optical behavior has been mostly investigated in quantum wells and self-organized embedded quantum dots (QDs) fabricated by molecular-beam heteroepitaxy (MBE) (e.g., Ge-Si, GaSb-GaAs, and ZnTe-ZnSe).[1,6–10,13,14] However, the energetic barriers in these nanostructures are usually lower than those attainable in colloidal QDs and heteroNCs, which are typically much smaller than their MBE counterparts. Moreover, colloidal chemistry methods are cheaper and easier to upscale than MBE techniques, and offer the additional advantages of processability and easier control over size, shape, and surface. The potential of colloidal type-II heteroNCs has attracted increasing attention over the last few years, leading to the investigation of heteroNCs of various compositions [viz., CdTe-CdSe,[15–20] CdSe-ZnTe,[21] and CdS-ZnSe (Refs. 2 and 22)] and shapes (viz., core/shell QDs,[2,15,19–22] heterorods and multipods,[15–17,21] and dumbbells[18]). Despite this booming activity and the great advances made in recent years, a thorough fundamental understanding of nanoscale spatially indirect excitons has yet to emerge.

Previous work on colloidal type-II heteroNCs focused mostly on the qualitative aspects of the absorption and photoluminescence (PL) spectra. The indirect exciton lifetime has been much less investigated, probably due to the low PL quantum yields (QYs) usually associated with type-II heteroNCs. The absorption cross section of the spatially indirect exciton has also received very little attention. Moreover, a systematic investigation comparing the absorption cross section and the radiative lifetime of indirect excitons is still lacking. In this work, we investigate the evolution of the optical properties of CdTe/CdSe heteroNCs upon increasing CdSe volume fraction, with emphasis on quantitative aspects, such as the absorption cross section of the lowest-energy exciton transition, the Stokes shift, transition linewidths, and the exciton radiative lifetime. CdTe/CdSe heteroNCs are chosen as a model system for a number of reasons. First, CdTe and CdSe QDs are model systems themselves, being the most investigated and best understood colloidal QDs. Recently, the size (and frequency) dependence of the spontaneous emission rate and of the absorption cross section of the $1S_{3/2(h)} \rightarrow 1S_{(e)}$ transition of CdSe and CdTe QDs has been systematically investigated over a wide size range.[23] The method reported in Ref. 23 makes it possible to follow the evolution of the absorption cross section of the lowest-energy exciton transition during the growth of CdTe/CdSe heteroNCs, and to compare it with the size- (and frequency-) dependent trends observed for CdTe and CdSe QDs.[23] Second, highly luminescent CdTe/CdSe colloidal heteroNCs have become recently available,[15] offering an ideal system for the investigation of the exciton radiative lifetimes. The results reported here provide fundamental insights into the size, shape, and composition dependence of nanoscale spatially indirect excitons in semiconductor heteroNCs.

This paper is organized as follows. First, the experimental methods are described, followed by a brief review of theoretical models for excitons in semiconductor heteronanostructures. Subsequently, the results are presented and discussed, starting with the qualitative trends observed in the optical properties with increasing CdSe volume fraction ($V_{fr(\mathrm{CdSe})}$). The hole localization in the CdTe core is demonstrated in the Sec. IV B. The Sec. IV C is dedicated to the assignment of the optical transitions observed in the absorption spectra and their evolution upon growth of the CdSe segment of the heteroNC. The evolution of the absorption cross section of the lowest-energy exciton transition, of the nonresonant Stokes shift, and of the transition linewidths is analyzed in the Sec. IV D. The room-temperature exciton lifetimes are addressed in the Sec. IV E, with emphasis on the observation of two radiative decay rates and their evolution with increasing $V_{fr(\mathrm{CdSe})}$. The temperature dependence of the PL spectra and of the PL decay curves in the 4–300 K range is discussed for a representative sample. Finally, in the last section, the trends observed for the radiative lifetimes and the absorption cross sections are compared.

II. EXPERIMENT

Synthesis and characterization. The colloidal CdTe/CdSe heteroNCs investigated in this work were prepared by a multistage seeded growth approach described in detail previously.[15] High-quality CdTe QDs (2.6 nm diameter, 5–10 % dispersion) were used as cores.[24] CdTe/ZnSe colloidal heteroNCs were grown for comparison, under the same conditions and from the same cores used for the CdTe/CdSe heteroNCs. Type-I core/shell/shell (CSS) QDs [viz., CdSe/ZnSe, CdSe/ZnSe/ZnS, and CdSe/(Cd,Zn)S/ZnS] were prepared following procedures described in the literature.[25,26] CdSe nanorods ($L=10.5\pm1.5$ nm, $d=2.9\pm0.3$ nm, and QY: 45%) capped with a very thin CdS shell (0.35 nm in the length direction only) were supplied by Dr. P. T. Chin.[27] Transmission electron microscopy (TEM) and high-resolution TEM (HRTEM) were performed on a TECNAI G 20 TE microscope (FEI Co., The Netherlands) operated at 200 kV or on a Titan Krios TE microscope (FEI Co., The Netherlands) operated at 300 kV.

Optical spectroscopy. Absorption, PL, and PL excitation (PLE) spectra were acquired as described before.[23] The spectra were corrected for the instrumental response and the spectral dependence of the excitation lamp intensity. Samples for optical measurements were prepared by directly dissolving the crude reaction mixture in anhydrous toluene under argon or nitrogen. In order to avoid reabsorption, energy transfer (ET) between the heteroNCs, and deviations from linearity in the absorption and PLE spectra, all optical measurements were carried out on samples with a low optical density ($\leq$0.05 at the lowest-energy absorption maximum and $\leq$0.2 at 3.1 eV). For low-temperature measurements, the sample was contained in a sealed quartz cuvette (optical path: 2 mm) and mounted in a continuous He-flow cryostat allowing for measurements down to 4.2 K.

PL QY were estimated by comparison with a standard, following a previously reported method,[28] as follows:

$$\mathrm{QY} = \left(\frac{1-T_{ST}}{1-T_X}\right) \times \left(\frac{\Delta\Phi_X}{\Delta\Phi_{ST}}\right) \times q_{ST}, \qquad (1)$$

where T_{ST} and T_X are the transmittances at the excitation wavelength λ_{exc} for the standard and the sample, respectively, and q_{ST} is the quantum yield of the standard. The terms $\Delta\Phi_X$ and $\Delta\Phi_{ST}$ give the integrated emitted photon flux

(photons s^{-1}) for the sample and the standard, respectively, upon excitation at λ_{exc}. The excitation wavelength is chosen such that both the sample and the standard are efficiently excited under exactly the same set of instrumental conditions. Ethanolic solutions of three different dyes (laser grade, Exciton Inc.) were used as standards: Rhodamine B, Rhodamine 101, and Rhodamine 6G (q_{ST}=90%, in all three cases). The values of $\Delta\Phi_X$ and $\Delta\Phi_{ST}$ are determined from the corrected PL spectra. Care was taken to ensure a constant and reproducible position for the sample/standard holder and unchanged instrumental conditions throughout the measurements. The accuracy of the method is ±10%.

The relative energy-integrated absorption cross section *per* ion-pair unit of the lowest-energy exciton transition (μ^*_{SS}) was obtained by determining the area of the lowest-energy peak in the PLE spectra (in energy scale) normalized at 3.1 eV,[23]

$$\mu^*_{SS} = \int_{\hbar\omega_1}^{\hbar\omega_2} (\mu_{\hbar\omega}/\mu_{3.1\ \mathrm{eV}}). \tag{2}$$

The normalization is equivalent to adjusting the volume fraction of semiconductor material in solution to be the same for all samples.[23] The mean deviation for the normalized absorption cross sections at 3.3 eV is smaller than 5%. In order to accurately determine the area of the lowest-energy peak, the PLE spectra were fit to a sum of multiple Gaussian bands ($\chi^2_r \geq 0.999$), using the minimum number of Gaussians needed to accurately describe the spectra. This constraint is particularly relevant for spectra showing the featureless low-energy tail characteristic of type-II heteroNCs (see below). The total-energy-integrated absorption cross section per ion-pair unit (μ^*_{TOT}) was obtained by integrating over all the exciton transitions from 3.1 eV to the absorption onset (viz., 1.4–2.2 eV, depending on the sample).

Nonresonant Stokes-shift values [$\Delta_{ST}(nr) = E^{\mathrm{PLE}}_{peak} - E^{\mathrm{PL}}_{peak}$] were obtained from PLE and PL spectra in energy scale. The peak positions for the lowest-energy absorption transition (E^{PLE}_{peak}) were determined by fitting the PLE spectra (in energy scale) to a sum of multiple Gaussian bands and taking the peak position of the lowest-energy band. The $\Delta_{ST}(nr)$ values are corrected for the offset between the emission and excitation monochromators.

PL decay curves were obtained by time-correlated single-photon counting via time-to-amplitude conversion, as previously described.[26] A Pico Quant PDL 800-B laser was used as the excitation source (λ_{exc}=406 nm, 55 ps pulse width, repetition rates: 0.2–20 MHz). Very low excitation fluences were used ($<0.5\ \mathrm{nJ/cm^2}$) in order to avoid multiexciton formation, and to keep the ratio of stop to start pulses below 0.04. The raw decay data were fitted to decay functions using a Simplex minimization algorithm implemented in PICOQUANT FLUOFIT 3.3. To allow consistent comparison between different samples, while ensuring that the obtained decay constants were statistically valid and representative of the whole heteroNC ensemble, the decay data were fit from I_0 (t=0) to $<1\%I_0$ (background level) using only three decay functions: single-exponential, biexponential, or Gaussian distribution. The fit quality was assessed by two criteria: reduced χ^2 ($\approx$1.0) and the weighed residuals' autocorrelation function (random distribution of small values).

III. THEORETICAL MODELS FOR EXCITONS IN SEMICONDUCTOR HETERONANOCRYSTALS

Excitons in embedded semiconductor QDs have been theoretically studied by, among others, Laheld and co-workers.[1] Their model is based on the effective-mass approximation and considers a spherical QD embedded in a matrix of a different semiconductor, with finite band offsets between the two materials. For simplicity, the dielectric constants of the two semiconductors are replaced by an average dielectric constant, and the same effective mass is assumed for the carriers inside the QD and in the matrix material. Three limiting localization regimes are identified depending on the band offsets between the QD and the matrix material:[1]

(a) *Type-I regime* (enclosed alignment, the band gap of the QD lies entirely within the gap of the matrix): both carriers are confined in the QD.

(b) *Type-II regime* (staggered alignment): carriers are spatially separated on different sides of the heterojunction. Complete spatial separation occurs only for the physically unrealistic case of infinite offsets. For finite offsets, the wave function of the confined carrier partially extends into the matrix material, leading to nonzero e-h wave-function overlap integrals Θ, which are predicted to decrease with increasing size until the QD becomes larger than the confined carrier Bohr radius. The carriers will then become spatially correlated and, consequently, the oscillator strength (proportional to Θ) will increase with the QD size.[1]

(c) *Type-$I^{1/2}$ regime* (zero offset for one carrier, finite offset for the other): one carrier is confined to the QD while the other is free. The Coulomb potential created by the confined carrier binds the free carrier so that they become spatially correlated.[1]

Excitons in colloidal core/shell QDs have been described using a similar model.[2,18,19,22] The essential difference is that the second semiconductor material is no longer an infinite matrix embedding the QD but rather a concentric shell of finite thickness, which is embedded in a dielectric medium. Consequently, photogenerated carriers will experience quantum confinement in both components of the heterostructure. An elaborated theoretical modeling, based on the effective-mass approximation and applying first-order perturbation theory to treat both electron-hole Coulomb coupling and interface polarization effects, has been recently performed by Klimov and co-workers.[2] Four limiting localization regimes are identified: "*type-I*" (both carriers are primarily localized in the core), "*inverted type-I*" (both carriers in the shell), "*quasi type-II*" (one carrier is confined to the core or shell while the other is delocalized over the whole heteronanocrystal), and "*true type-II*" (spatially separated carriers, i.e., the wave functions of the electron and of the hole reside largely on different sides of the heterojunction).

The electronic structure of colloidal semiconductor heterostructures has also been modeled by applying different methodologies, such as, e.g., the few-band $\mathbf{k}.\mathbf{p}$ approximation, tight-binding, and empirical pseudopotential

TABLE I. Main characteristics of representative colloidal CdTe/CdSe heteronanocrystal samples. Photoluminescence peak (PL peak), PL quantum yield (QY), heteroNC dimensions, heteroNC volume (V_{NC}), volume fraction of CdSe in the heteroNC ($V_{fr(CdSe)}$), and dimensions of the CdSe part of the heteroNC along the length and diameter directions, assuming that the CdTe core occupies the center of the heteroNC.

Sample	PL peak (eV)	QY (%)	HeteroNC dimensions[a] (nm)		V_{NC} (nm^3)	$V_{fr(CdSe)}$ (%)	CdSe dimensions[a] (nm)	
			Length	Diameter			Length direction	Diameter direction
1%CdSe	2.277	34	2.8 ± 0.3	2.6 ± 0.3	9.3	1	0.2[b]	
21%CdSe	2.119	45	3.94 ± 0.50	2.7 ± 0.4	11.7	21	0.66	0.1
39%CdSe	1.971	80	4.44 ± 0.45	3.1 ± 0.4	15.0	39	0.92	0.2
52%CdSe	1.755	79		5.2 ± 0.4 [c]	19.0	52	1.3[d]	
88%CdSe	1.610	75	8.0 ± 1.6 [e]	2.9 ± 0.3 [e]	80	88	6.7[f]	3[f]

[a]The CdTe core is the same in all cases (diameter: 2.6 ± 0.3 nm).
[b]Tips.
[c]Trigonal pyramids.
[d]Diagonal direction.
[e]Sample consists mostly of bipods.
[f]Arm length and diameter.

approaches.[4,22] Recently, Zunger and co-workers carried out calculations of the electronic states of CdTe/CdSe/CdTe nanodumbbells [QD/Qrod(QR)/QD] by combining an atomistic single-particle local-density approximation approach with a configuration-interaction many-particle method.[4] The diameter of the CdTe QDs (5 nm) and length of the CdSe QR (3 nm) were kept constant. Three limiting electron localization regimes are observed depending on the CdSe QR diameter. The hole wave function is localized on the CdTe QDs, regardless of the dumbbell geometry.[4] In the case of a narrow rod ($d=1.6$ nm), the lowest-energy state of the electron is localized on the CdTe QDs while in a wide rod ($d=3$ nm), the electron is primarily localized in the CdSe QR as a result of the reduced quantum confinement. Interestingly, the CdTe QD and CdSe QR electron states are strongly coupled in the case of an intermediate diameter rod (2 nm), and, consequently, the lowest-energy electron state is delocalized over the whole nanodumbbell.

We note that, despite the different theoretical methodologies and terminologies, the three limiting cases identified by Zunger and co-workers[4] are analogous to the localization regimes proposed by both Klimov and co-workers[2] and Laheld and co-workers.[1] Further, the *quasi type-II* and the "type-$I^{1/2}$" regimes are equivalent. In this work, we will favor the terminology proposed by Laheld and co-workers.[1] However, one should keep in mind that this terminology refers to *limiting* localization regimes, which are strictly true only for the physically unrealistic case of infinite offsets. For finite offsets, the boundaries between the three regimes are not sharply defined, particularly in nanoscale systems. As mentioned above, there is no true charge-carrier separation in quantum-confined nanoscale heterostructures since the electron and hole wave functions will partly extend across the heterojunction in all three localization regimes. Therefore, when applied to heteronanostructures, the localization regimes defined above[1,2] should be interpreted as meaning that the wave function of a given carrier largely resides on one particular material (type-I or type-II, depending on whether both carriers are primarily confined in the same material or in different materials, respectively), or rather is delocalized over the whole heteroNC (type-$I^{1/2}$). The extent to which the confined wave functions will spread over the heterojunction depends on the potential barrier at the interface, being more pronounced for smaller energy offsets.[1,2] However, the energy offsets across nanoscale heterojunctions are not *a priori* known, and are difficult to directly determine, even when the bulk band offsets are known. Therefore, in the present work, we will use spectroscopic signatures to identify the localization regime of the electron and hole wave functions in CdTe/CdSe heteroNCs.

IV. RESULTS

A. Optical properties of CdTe/CdSe heteroNCs: Qualitative trends

Table I presents the main characteristics of a set of representative CdTe/CdSe heteroNC samples. It should be pointed out that these samples are the same as those previously reported in Ref. 15 (samples A, B, C, D, and E, respectively). However, the optical properties of these samples (viz., absorption, PL and PLE spectra, PL QYs, and PL decay curves) have been reinvestigated in the present work. TEM images for some of these samples are presented in Fig. 1. The CdSe growth is highly anisotropic, initially yielding prolate CdTe/CdSe core/shell heteroNCs, which evolve into trigonal pyramids and then into multipods of increasing complexity (initially mostly bipods, tetrapods become dominant at later growth stages).[15]

The evolution of the optical properties upon growth of the CdSe part is illustrated in Fig. 2. The heteroNC volume and the CdSe volume fraction $V_{fr(CdSe)}$ are better suited as variables to follow the changes in the optical properties since the shape of the heteroNCs is anisotropic and continually changes during the growth. The PL peak shifts to lower energies with increasing $V_{fr(CdSe)}$ (Fig. 2 and Table I). The re-

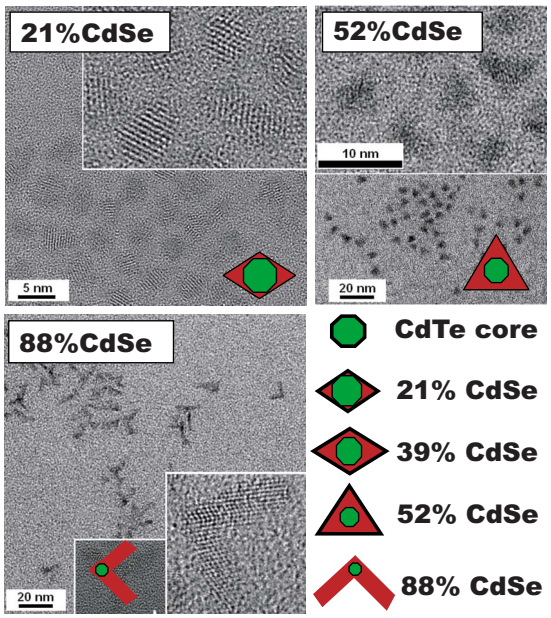

FIG. 1. (Color online) Overview TEM images of selected CdTe/CdSe heteronanocrystal samples with a 2.6 nm CdTe core and increasing CdSe volume fraction ($V_{fr(\mathrm{CdSe})}$). Insets show corresponding HRTEM images. Labels correspond to Table I. The lower right panel shows a schematic of the shape evolution of the heteroNCs with increasing $V_{fr(\mathrm{CdSe})}$ (drawings are not to scale).

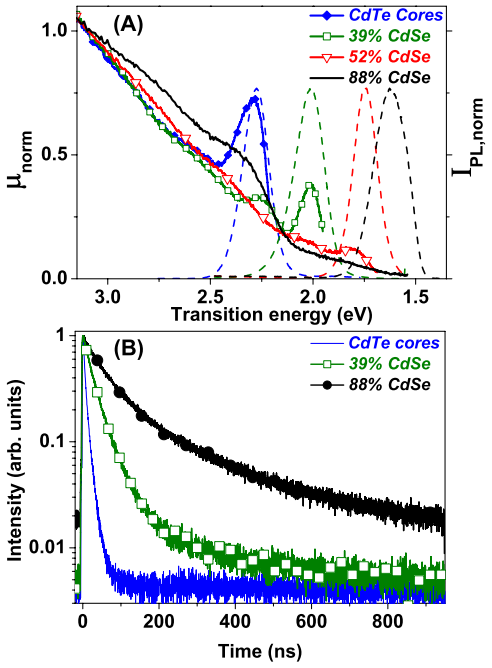

FIG. 2. (Color online) Optical properties of representative colloidal CdTe/CdSe heteroNCs with a 2.6 nm CdTe core and increasing CdSe volume fraction. Data are also shown for the CdTe core. Labels correspond to Table I. (A) PL (dashed lines) and PLE (solid lines) spectra. PLE spectra are normalized to 1 at 3.1 eV. μ_{norm} gives the normalized absorption cross section per Cd(Te,Se) ion-pair unit. The PL spectra are normalized at the peak. (B) PL decay curves.

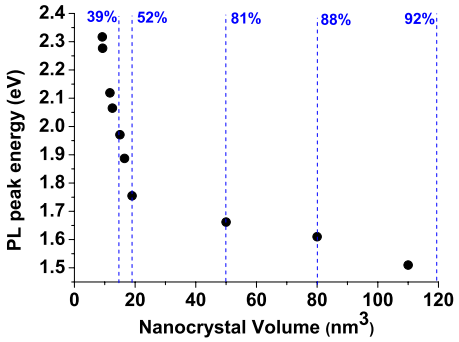

FIG. 3. (Color online) PL peak energy as a function of the nanocrystal volume for CdTe/CdSe heteroNCs with a 2.6 nm CdTe core and increasing CdSe volume fraction ($V_{fr(\mathrm{CdSe})}$). The first data point corresponds to the bare CdTe core. The dashed lines give the $V_{fr(\mathrm{CdSe})}$ values for selected volumes.

lationship between the PL energies and the volume of the heteroNCs is conveyed in Fig. 3. It is clear that the dependence is much less pronounced after the onset of branching, most likely because the increase in volume is then primarily due to the increase in the number and length of the arms.

The absorption (and PLE) spectra also shift to lower energies with increasing $V_{fr(\mathrm{CdSe})}$ (Figs. 2 and 4). Initially, the absorption peaks remain well defined and distinct but eventually a featureless absorption tail develops as the $V_{fr(\mathrm{CdSe})}$ increases. Similar observations have been reported for a number of core/shell type-II heteroNCs.[2,15,19–22] The indis-

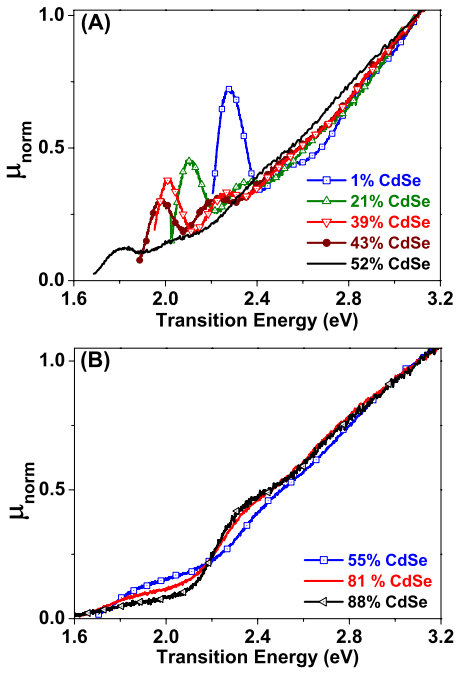

FIG. 4. (Color online) PL excitation spectra of colloidal CdTe/CdSe heteroNCs with a 2.6 nm CdTe core and increasing CdSe volume fraction in the (A) type-$I^{1/2}$ (1–52 % CdSe volume fraction, from right to left, respectively) and (B) type-II (55–90 % CdSe volume fraction, from top to bottom, respectively) carrier localization regimes. The spectra are normalized to 1 at 3.1 eV. μ_{norm} gives the normalized absorption cross section per Cd(Te,Se) ion-pair unit.

tinct absorption tail is regarded as a clear signature of a spatially indirect exciton transition.[2,15,19–22] A qualitative explanation for the observed trends and a tentative assignment for the transitions will be provided below (Sec. IV C). The redshift of the transitions is accompanied by a decrease in the absorption cross section of the lowest exciton transition and an increase in the exciton lifetimes (Fig. 2). A detailed analysis of the evolution of the absorption cross sections and exciton radiative lifetimes will be provided later in this paper (Secs. IV D and IV E, respectively).

The high PL QY of the samples implies that the contribution of nonradiative recombination in surface or heterojunction defects is small, and therefore that the PL decay curves are dominated by the exciton radiative recombination. These heteroNCs are thus ideal systems to study the intrinsic exciton dynamics and to extract the indirect exciton radiative lifetimes. It is worth noting that the heteroNCs investigated here are grown under conditions at which interfacial alloying is expected to be negligible (viz., low temperatures and alternate precursor additions).[15] To check whether this assumption is justified, CdTe/ZnSe heteroNCs were grown under the same conditions used for the CdTe/CdSe heteroNCs and from the same CdTe cores. Only a minor PL redshift (50 meV) was observed after addition of three monolayers of ZnSe, consistent with the expected type-I band alignment. This shows that unintentional interfacial alloying due to interdiffusion is negligible since alloying would induce much larger red shifts.[29]

B. Hole localization in CdTe/CdSe heteroNCs

The temperature dependence of the PL spectra and of the PL decay curves of colloidal CdTe/CdSe heteroNCs upon heating from 293 to 400 K has been reported in detail in Ref. 15. Thermally induced PL quenching is significantly reduced already for small CdSe additions (viz., 1% $V_{fr(\mathrm{CdSe})}$) and is absent for larger $V_{fr(\mathrm{CdSe})}$, in contrast with the behavior of CdTe QDs (and also CdSe QDs and CdSe/ZnS core/shell QDs).[15] This observation is remarkable and suggests that at least one of the charge carriers is confined to the CdTe core and no longer significantly probes the surface. Considering that a comparative study has shown that CdTe/CdSe core/shell QDs show efficient PL at room temperature[29] whereas the reversed CdSe/CdTe core/shell QDs hardly show any emission, it can be concluded that the PL quenching in these systems is largely due to hole trapping at surface sites. Therefore, the absence of thermally induced PL quenching for the CdTe/CdSe heteroNCs investigated here implies that the hole wave function is confined to the CdTe core already for small $V_{fr(\mathrm{CdSe})}$. Nevertheless, for $V_{fr(\mathrm{CdSe})}$ smaller than $\sim$20%, the heteroNC surface is not yet fully covered by CdSe, and therefore the hole may still significantly probe the surface. Further, the PL band of the CdTe/CdSe heteroNCs shifts to lower energies with increasing temperature.[15] This thermally induced PL shift is ascribed to the temperature dependence of the band gap, which is more pronounced for CdTe than for CdSe.[15] Therefore, the observation that the thermally induced redshift decreases with increasing $V_{fr(\mathrm{CdSe})}$ implies that the emitting state has an increasingly larger contribution of the CdSe component. This suggests that the electron wave function delocalizes over the whole heteroNC (i.e., type-$\mathrm{I}^{1/2}$ regime) already for small $V_{fr(\mathrm{CdSe})}$ and then progressively increases its amplitude in the CdSe part with further growth.

To probe the amplitude of the hole wave function at the surface of the heteronanocrystals, an excess of hexanethiol (HT) was added to solutions of CdTe/CdSe heteroNCs (viz., samples 1%CdSe, 21%CdSe, 39%CdSe, and 88%CdSe). Thiol groups can very efficiently trap photogenerated holes in CdSe QDs, thereby quenching the excitonic emission.[30,31] The HT-induced quenching is very efficient and is virtually complete for concentrations above 1×10^3 HT molecules/QD.[32] In the present study, a concentration as high as 5×10^5 HT molecules/heteroNC was used. To prevent effects due to photochemical reactions, the PL spectra was measured 2 min after the HT addition and with very short acquisition times (viz., 2 s). Although HT molecules have been reported to enhance the PL efficiency of CdTe QDs after 1 day of equilibration,[30] the short-time range after thiol addition has not yet been studied. Therefore, two samples of CdTe QDs (3.0 and 4.5 nm in diameter) were also investigated for comparison. The results revealed that in the short-time regime (viz., $<$10 min), the PL of CdTe QDs is also quenched by a large excess of HT molecules. The PL quenching is not as pronounced as that reported for CdSe QDs (Ref. 32) but is substantial (viz., 50% and 27%, for 3 nm and 4.5 nm in diameter, respectively). The decrease in the PL intensity is accompanied by a small redshift (12 meV and 2 meV for 3 nm and 4.5 nm in diameter, respectively), which clearly shows that the HT molecules have attached to the CdTe surface.[33]

The effect of adding an excess of HT molecules to CdTe/CdSe heteroNCs is remarkably different from that observed for the CdTe QDs. A redshift of the PL peak was also observed (viz., 40 meV for 1%CdSe and 21%CdSe, 20 meV for 39%CdSe and 88%CdSe) but was accompanied by an enhancement of the PL intensity, rather than by quenching (viz., 21%, 12%, and 5% for samples 1%CdSe, 21%CdSe, and 39%CdSe, respectively). Only sample 88%CdSe showed a modest decrease in the PL intensity (viz., 8%). Sample 88%CdSe was also purified (i.e., excess of unbound surfactants was removed) by precipitation and redispersion in toluene prior to adding HT. This should facilitate quenching by HT molecules but nevertheless the same minor effect was observed (viz., no changes in the absorption spectrum and in the exciton lifetimes, and only a 10% decrease in the PL intensity accompanied by a 20 meV redshift). Considering the large $V_{fr(\mathrm{CdSe})}$ of this heteroNC (viz., 88%), these observations clearly demonstrate that the hole is confined to the CdTe core.

The redshift observed in the PL spectra upon HT addition shows that the amplitude of the electron wave function at the surface of the heteroNCs is substantial since this shift can be ascribed to a strong coupling between the sulfur atoms bound to the surface Cd sites and the photoexcited electron. This leads to a partial expansion of the electron wave function into the surfactant shell,[33] which is more pronounced for the smaller heteroNCs due to the stronger quantum confinement. The observation of PL enhancement rather than quenching

clearly shows that hole trapping by HT molecules is inefficient, in striking contrast with the behavior exhibited by both CdTe and CdSe QDs. This suggests that the amplitude of the hole wave function at the surface is already significantly reduced by small $V_{fr(\mathrm{CdSe})}$, implying that the hole wave function does not substantially extends into the CdSe segment of the heteroNC, regardless of its volume. Nevertheless, as mentioned above, the surface coverage provided by small CdSe volume fractions (<20%) is incomplete, and, consequently, the hole should still probe the (CdTe) surface for sample 1%CdSe, making trapping possible. This is in contrast with the observations described above and suggests that at least part of the surface Te^{2-} ions may have been exchanged by Se^{2-} ions. This would not lead to an observable size change but would decrease the hole wave-function density at the surface, accounting for the reduced hole trapping rates. The observed PL enhancement is inversely correlated with the PL QYs of the heteroNCs (i.e., samples with lower PL QYs show larger enhancements), showing that the HT molecules remove electron traps by binding to surface Cd^{2+} ions.

We note that purification by precipitation and redispersion did not affect the optical properties of the CdTe/CdSe heteroNCs, in contrast with single-component CdTe and CdSe QDs (Ref. 23) but consistent with the behavior of core/shell QDs.[25] This clearly illustrates that recombination in surface states is negligible for the heteroNCs with $V_{fr(\mathrm{CdSe})} \geq 20\%$, in line with their high PL QYs. The thiol addition experiments described above clearly demonstrate that the hole wave function remains confined to the CdTe core as the CdSe segment of the heteroNC grows while the amplitude of the electron wave function at the surface remains substantial, regardless of the CdSe volume fraction.

C. Evolution of the absorption transitions

PLE spectra are better suited than absorption spectra for the identification and assignment of absorption transitions. First, only the emitting heteroNCs contribute to the PLE spectra while the absorption spectra contains contributions from all absorbing species in the volume sampled (i.e., nonemitting heteroNCs, impurities, surfactants, etc.). Second, the PLE technique allows a narrow portion of the ensemble of emitting heteroNCs to be spectrally selected, thereby minimizing the impact of size and shape inhomogeneities. Another useful feature of the PLE technique is that the comparison of PLE and absorption spectra allows the presence of nonemitting species to be detected and contributions from different emitting species to be distinguished. For the CdTe/CdSe heteroNCs investigated in this work, a close correspondence is observed between the PLE and the absorption spectra. This shows that all photoexcitation energy absorbed across the entire range from ~3.2 eV to the absorption onset of the heteroNCs (viz., 1.4–2.2 eV, depending on the sample) results in the population of exciton states that efficiently relax to the emitting state. This shows that competing absorption by byproducts of the synthesis (e.g., homogeneously nucleated CdSe NCs, bare CdTe QDs) is negligible.

The absorption transitions observed for the CdTe cores (Fig. 2) can be assigned by analogy with those observed for CdSe QDs (Ref. 34) since the two semiconductors are very similar: $1S_{3/2(h)} \rightarrow 1S_{(e)}$ (2.25 eV); $2S_{3/2(h)} \rightarrow 1S_{(e)}$ (2.6 eV), and $1P_{3/2(h);1/2(h)} \rightarrow 1P_{(e)}$ (2.9 eV). The absorption transitions remain well defined and distinct while shifting to lower energies, up to ~50% $V_{fr(\mathrm{CdSe})}$ [Figs. 2(A) and 4(A)]. As shown above, the hole wave function remains confined to the CdTe core during the heteroNC growth. This implies that the observed transitions are from the hole levels of the CdTe core, which remain undisturbed by the CdSe overgrowth. The redshift of the absorption transitions is thus primarily due to a loss in electron confinement energy, which indicates that the lowest-energy electron state is delocalized over the whole heteroNC (i.e., the NCs are in the type-$I^{1/2}$ regime). We will refer to this state as $1S_e$(hetero). Since the hole levels have not changed and the $1S_e$(hetero) is a coherent state delocalized over the whole heteroNC, the absorption transitions remain direct, and therefore distinct and well defined. The discrete features observed for the CdTe/CdSe heteroNCs in the type-$I^{1/2}$ regime can be thus ascribed to the following absorption transitions (energies refer to samples 39%CdSe and 52%CdSe, respectively): $1S_{3/2(h)}(\mathrm{CdTe}) \rightarrow 1S_{(e)}(\mathrm{hetero})$ (2.03 and 1.82 eV); $2S_{3/2(h)}(\mathrm{CdTe}) \rightarrow 1S_{(e)}(\mathrm{hetero})$ (2.25 and 2.06 eV); $1P_{(h)}(\mathrm{CdTe}) \rightarrow 1P_{(e)}(\mathrm{hetero})$ (2.6 and 2.45 eV); and $3S_{1/2(h)}(\mathrm{CdTe}) \rightarrow 1S_{(e)}(\mathrm{hetero})$ (2.9 and 2.8 eV).

The $1S_{(e)}(\mathrm{CdSe})$ state [or its equivalent in nanorods, $1\Sigma_{(e)}(\mathrm{CdSe})$] progressively shifts to lower energies as the volume of the CdSe part increases, until it becomes the lowest-energy state for the electron. The lowest-energy absorption transition will then be the spatially indirect transition $1S_{3/2(h)}(\mathrm{CdTe}) \rightarrow 1S_{(e)}(\mathrm{CdSe})$ [or $1S_{3/2(h)}(\mathrm{CdTe}) \rightarrow 1\Sigma_{(e)}(\mathrm{CdSe})$ in branched heteroNCs, such as sample 88%CdSe], giving rise to the featureless low-energy tail characteristic of type-II heteroNCs [Fig. 4(B)]. Intraband spectroscopic measurements on a number of type-II QDs (viz., CdS/CdSe; CdS/ZnSe) has demonstrated that the hole and the electron levels of the different components remain discrete,[22] leading to sharp and well-defined features in the intraband spectra, despite the featureless and broad interband spectra. The absence of distinct features in the low-energy absorption tail is thus a consequence of the spatially indirect nature of the transition(s) involved. Spatially indirect exciton transitions involve states in different materials (e.g., the $1S_{3/2(h)}$ of CdTe and the $1S_{(e)}$ of CdSe). These states are not only offset in real space but are also defined with respect to different sets of k wave vectors (i.e., two independent Brillouin zones, each with its own origin in k space, see Fig. 5 for a schematic representation). Therefore, the energy dispersion in k space of the electron and hole states involved in the transition becomes relevant, leading to broadening of the transition bandwidth, which progressively increases as the spatial dimensions of the components of the heteroNC increase [Fig. 4(B)]. As it will be shown in the next section, this also leads to a larger relaxation after photoexcitation, which is reflected in larger Stokes-shift values. Nevertheless, the transition from type-$I^{1/2}$ to type-II is not abrupt, due to the mixing between the close-lying $1S_e$(hetero) and the $1S_{(e)}$(CdSe) states, which gradually decreases as the energy difference between the states increases due to the shift of the $1S_{(e)}$(CdSe) state [or $1\Sigma_{(e)}$(CdSe)] to lower energies.

Besides the indirect exciton absorption tail between 2.06 and 1.55 eV, the spectrum of sample 88%CdSe [Figs. 2(B)

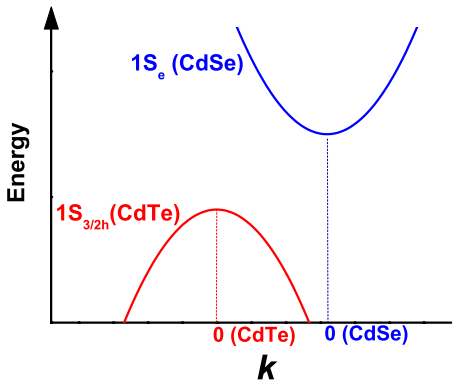

FIG. 5. (Color online) Schematic energy-level diagram for CdTe/CdSe heteroNCs in the type-II regime. For simplicity only the lowest-energy states for the electron and hole are represented. The energy dispersion in k space is taken to be parabolic. Note the different origins (k=0) for CdTe and CdSe.

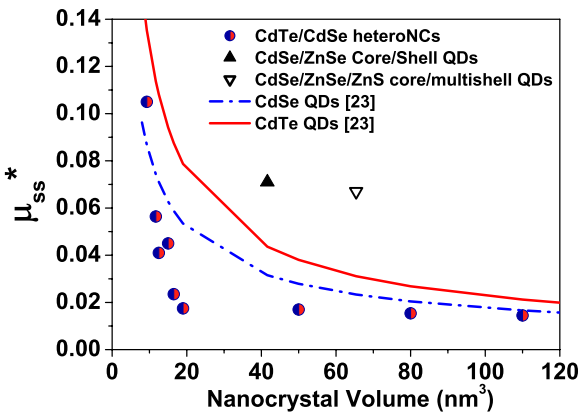

FIG. 6. (Color online) Relative energy-integrated absorption cross section per ion-pair unit of the lowest-energy exciton transition (μ^*_{SS}) as a function of the nanocrystal volume for CdTe/CdSe heteroNCs with a 2.6 nm CdTe core and increasing CdSe volume fraction. Data for CdSe/ZnSe and CdSe/ZnSe/ZnS core/shell QDs are also included. The lines give the empirical trends reported in the literature for the $1S_{3/2(h)} \rightarrow 1S_{(e)}$ transition of CdSe and CdTe QDs (Ref. 23).

and 4(B)] also shows broad peaks at higher energies (viz., 2.3 and 2.7 eV). Similar features are also observed in the PLE spectra of other samples in the type-II regime (e.g., peaks at 2.4 and 2.8 eV for sample 55%CdSe, Fig. 4). The assignment of these peaks, however, is not straightforward since direct transitions in the CdSe arms are also expected in this spectral region.[35,36] Investigations on CdSe/CdTe heteronanorods have shown that the redshift for the direct transitions in the CdSe part of the heterorods is negligible with respect to those in CdSe nanorods of similar dimension.[16] Therefore, since the energy-level structure of CdSe nanorods depends primarily on the diameter of the nanorod, rather than on its length,[35] literature values for direct exciton transitions in CdSe nanorods can be used to help identifying similar transitions in the type-II CdTe/CdSe heteroNCs investigated here, provided the diameters are comparable. The CdSe arm is longer for sample 88%CdSe than for sample 55%CdSe (viz., 7 nm and 4 nm, respectively) but the arm diameter is the same (3 nm). The $1\Sigma_{1/2(h)} \rightarrow 1\Sigma_e$ and $1\Pi_{1/2(h)} \rightarrow 1\Pi_e$ transitions of CdSe nanorods with 2.9 nm diameter and 10.5 nm length have been observed at 2.2 eV and 2.65 eV, respectively.[27] The blueshift expected for nanorods with 2.9 nm diameter and 4 nm length is only 0.05 eV,[36] placing these transitions at 2.25 and 2.70 eV. These energies are considerably lower than the peak positions observed for sample 55%CdSe, suggesting that other indirect exciton transitions are also contributing to the PLE spectra of the type-II CdTe/CdSe heteroNCs investigated here [Figs. 2(B) and 4(B)].

The position of higher energy spatially indirect exciton transitions can be estimated from the peak position of the $1S_{3/2(h)}$(CdTe) $\rightarrow 1\Sigma_{(e)}$(CdSe) transition (viz., 1.85 eV and 1.9 eV, for samples 88%CdSe and 55%CdSe, respectively), and the relative positions of the CdTe hole states determined from the PLE spectra of the CdTe/CdSe heteroNC samples in the type-I$^{1/2}$ regime. This places the $2S_{3/2(h)}$(CdTe) $\rightarrow 1\Sigma_{(e)}$(CdSe) transition at 2.1 eV and 2.15 eV for samples 88%CdSe and 55%CdSe, respectively, consistently with the observation that two Gaussians are needed to fit the low-energy absorption tail in these samples (maxima at 1.85 and 2.05 eV for 88%CdSe, and 1.9 and 2.1 eV for 55%CdSe). The $3S_{1/2(h)}$(CdTe) $\rightarrow 1\Sigma_{(e)}$(CdSe) transition is estimated at 2.72 eV and 2.8 eV for samples 88%CdSe and 55%CdSe, respectively, in good agreement with the peaks observed in the PLE spectra of these samples. The peak at 2.4 eV in the PLE spectrum of sample 55%CdSe can be assigned to the $1P_{(h)}$(CdTe) $\rightarrow 1P_{(e)}$(hetero) transition. This transition is observed at 2.45 eV for sample 52%CdSe [Figs. 2(B) and 4(A)], which is still in the type-I$^{1/2}$ regime. Given the small $V_{fr(\mathrm{CdSe})}$ difference between these two samples it is reasonable to assume that the $1P_{(e)}$ state is still delocalized over the whole heteroNC. This assumption is supported by both theoretical modeling[19] and experimental results,[22] which have shown that thicker shells are required to localize the $1P_{(e)}$ state in type-II core/shell QDs.

D. Absorption cross sections, Stokes shift, and linewidths

1. Volume dependence of the absorption cross section

Figure 6 gives the volume dependence of the relative energy-integrated absorption cross section per ion-pair unit of the lowest-energy exciton transition (μ^*_{SS}) of CdTe/CdSe heteroNCs with increasing $V_{fr(\mathrm{CdSe})}$ and constant CdTe volume. The relative absorption cross sections per heteroNC (σ^*_{SS}) can be obtained from μ^*_{SS} and the number of ion-pair units per heteroNC ($\sigma^*_{SS}=\mu^*_{SS}N_{units/\mathrm{QD}}$).[23] Absolute μ_{SS} and σ_{SS} values can easily be obtained from the relative values by using bulk optical constants,[23] but this is not necessary to unravel the absolute trends, since the absorption cross section at 3.1 eV ($\mu_{3.1\ \mathrm{eV}}$) is constant and size independent.[23] The μ^*_{SS} values of CdTe/CdSe heteroNCs can be directly compared to those of CdTe and CdSe QDs (Fig. 6) because $\mu_{3.1\ \mathrm{eV}}$ is the same for bulk CdSe and CdTe.[23] Figure 6 also gives μ^*_{SS} values for type-I CSS QDs (CdSe/ZnSe and CdSe/ZnSe/ZnS), which can be compared to CdSe QDs because the ZnSe and ZnS parts do not contribute to $\mu_{3.1\ \mathrm{eV}}$. The band gap of bulk ZnS is 3.68 eV. The band gap of bulk ZnSe

is 2.80 eV but quantum confinement will shift the absorption of the 0.8-nm-thick ZnSe shell to higher energies (ZnSe QDs with $d<3$ nm absorb above 3.35 eV, Ref. 37). CdSe/CdS/ZnS CSS QDs cannot be directly compared to the other NCs shown in Fig. 6 because the CdS part contributes to $\mu_{3.1\ \mathrm{eV}}$ (CdS QDs with $d=2$ nm already absorb at 2.95 eV, Ref. 38).

The absorption cross section of an exciton transition is proportional to the transition oscillator strength and therefore to the absorption transition rate Γ_{SS}^{ABS},[23,39]

$$\Gamma_{SS}^{ABS} = \frac{2e^4 n}{\pi\varepsilon_0 m_0^3 \varpi_{SS} c^3} |F_{loc}|^2 \left[\frac{2m_0 \omega_{SS} \Theta P^2}{3e^2\hbar}\right], \qquad (3)$$

where e is the electron charge, m_0 the electron rest mass, ε_0 the permittivity of free space, c the speed of light, n the refractive index, F_{loc} is the local-field correction factor $(3\varepsilon_m/\varepsilon_1+2\varepsilon_m$, where ε_m is the dielectric constant of the surrounding medium and ε_1 is the dielectric constant of the semiconductor), and ω_{SS} is the transition frequency. The term Θ represents the square of the overlap integral between the electron and the hole envelope wave functions, and P is the Kane interband matrix element, $|\langle 1S_h|p|1S_e\rangle|$, which gives the transition electric dipole (ED) moment. The terms between square brackets define the oscillator strength f_{SS} for the transition.[39] The observation that the μ_{SS}^* values of CdTe/CdSe heteroNCs are much smaller than those for similarly sized CdSe or CdTe QDs (Fig. 6) implies a reduction in Θ with increasing heteroNC volume (and thus with increasing $V_{fr(\mathrm{CdSe})}$) since all other terms in Eq. (3) will remain essentially constant. The interband matrix element depends only on the chemical composition and crystal lattice (i.e., on the Bloch functions) and is very similar for CdTe and CdSe.[23] The changes in F_{loc} due to the different dielectric constants of CdSe and CdTe (viz., 7.8 and 9, respectively) can be neglected.[23] The e-h wave-function overlap integral Θ can be taken as a measure of the degree of spatial separation between electron and hole.[1,2,18,19] These observations are thus consistent with the formation of type-I$^{1/2}$ and type-II heteroNCs, corroborating the qualitative analysis presented above. The formation of type-I heteroNCs can be excluded because this would result in larger μ_{SS}^* values than those of similarly sized single-component QDs, as clearly illustrated by the type-I CSS QDs in Fig. 6.

The fact that the μ_{SS}^* values for the type-I CSS QDs are much larger than expected based on their sizes demonstrates that the relevant quantity is not the heteroNC volume but rather the "effective exciton volume." In quasispherical single-component QDs, the effective exciton volume is equivalent to the NC physical volume but for anisotropic or complex-shaped semiconductor NCs, the effective exciton volume can differ considerably from the physical volume.[40] For heteroNCs, the situation is more complex because the effective exciton volume will depend on the extent to which the exciton wave function of the core material spreads in the surrounding shell material. This is clearly illustrated by the type-I CSS QDs presented in Fig. 6. In type-I CSS QDs, the exciton is strongly confined in the core so that its effective volume is only slightly larger than that of the original cores (viz., 12 nm^3 for the CSS QDs shown in Fig. 6). However,

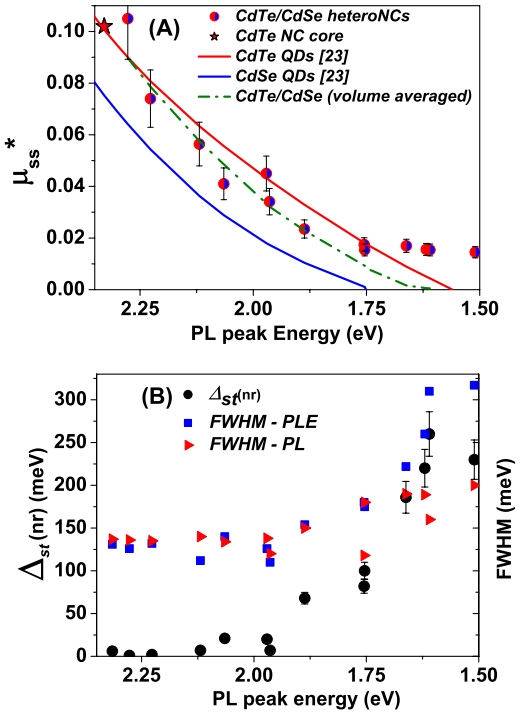

FIG. 7. (Color online) (A) Relative energy-integrated absorption cross section per ion-pair unit of the lowest-energy exciton transition (μ_{SS}^*) and (B) nonresonant Stokes shift [$\Delta_{ST}(nr)$] and full width at half maximum of the emission band (FWHM-PL) and of the lowest-energy excitation transition (FWHM-PLE), as a function of the PL peak energy for CdTe/CdSe heteroNCs with a 2.6 nm CdTe core and increasing CdSe volume fraction. The solid lines in (A) give the empirical trends reported in the literature (Ref. 23) for the $1S_{3/2(h)} \rightarrow 1S_{(e)}$ transition of CdSe (lower line) and CdTe (upper line) QDs. The dashed line in (A) gives the average between the μ_{SS}^* values for CdTe and CdSe QDs, considering the volume fractions of CdTe and CdSe in the heteroNCs.

the effective exciton volume is difficult to determine. The PL frequency (or energy) is a convenient surrogate variable to allow comparison between heteroNCs of different shapes, sizes, and compositions, as it can be determined with a much larger accuracy and reproducibility than the heteroNC size.[23] Further, the PL energy is determined by the electron and hole wave functions and is therefore directly related to the effective exciton volume. In this sense, the use of the PL frequency as a surrogate variable effectively normalizes the observed trend for the variation in the unknown effective exciton volume. Figure 7 presents μ_{SS}^*, the full width at half maximum for the emission and for the lowest-energy excitation bands (FWHM-PL and FWHM-PLE, respectively), and the nonresonant Stokes shift, $\Delta_{ST}(nr)$, for CdTe/CdSe heteroNCs with increasing $V_{fr(\mathrm{CdSe})}$, as a function of the PL peak energy. Before discussing the correlations between the trends observed in Fig. 7 and the implications of these observations, each parameter will be addressed separately.

2. Evolution of the transition linewidths

The linewidths of exciton transitions in ensembles of QDs are determined by both homogeneous and inhomogeneous

broadening contributions. The inhomogeneous broadening depends on the size (and shape) distribution in the ensemble while the homogeneous broadening gives the intrinsic transition linewidth and is determined by exciton dephasing.[41,42] A recent study has reported that the FWHM of the PL bands of CdSe QDs in the 3–8 nm diameter range (10% dispersion) varies from 120 to 80 meV at 300 K.[42] In the present work, we observe similar linewidths for both CdSe and CdTe QDs (150–80 meV in the 2.6–5 nm size range, 5–10 % size dispersion). The increase in linewidth observed upon decreasing size (under constant size dispersion) reflects the stronger quantum confinement experienced by excitons in smaller QDs. Larger size distributions result in larger inhomogeneous broadening. For example, the FWHM of CdSe QDs with an average diameter of 4.5 nm increases from 80 to 120 meV for an increase in size dispersion from 4% to 10%, respectively. CSS QDs typically show larger FWHM (viz., 100 ± 10 meV, for 1–3 nm thick shells over a 3 nm core) than single-component QDs, probably due to interfacial composition fluctuations. Considering the points above, it is clear that the trend observed in Fig. 7 for the FWHM values of CdTe/CdSe heteroNCs cannot be explained solely by an increase in the inhomogeneous broadening since the size dispersions deduced from the TEM measurements are not sufficiently large and do not significantly increase during the CdSe overgrowth (see Table I). The change in shape can also not explain the trend, given that the linewidths for nanorods are not significantly larger than those observed for QDs (e.g., 125 meV for CdSe nanorods with $L=10.5 \pm 1.5$ nm and $d=2.9 \pm 0.3$ nm). The increase in the FWHM of both emission and excitation bands can thus be taken to reflect the broadening of the intrinsic transition linewidths. It should be noted that the FWHM values for CdSe, CdTe, and type-I CSS QDs do not significantly differ for emission and excitation. In this context, it is of particular significance that the difference between the FWHM values for PL and PLE remains very small for the CdTe/CdSe heteroNCs in the type-$I^{1/2}$ regime but increases considerably after the onset of the features associated with type-II behavior. As discussed above, the more pronounced increase observed for the FWHM-PLE of the CdTe/CdSe heteroNCs in the type-II regime reflects the spatially indirect nature of the lowest exciton transition.

3. Evolution of the Stokes shift

The term "Stokes shift" has been used in the field of semiconductor NCs in a rather liberal way, which resulted in a number of related terms (viz., "resonant Stokes shift," "nonresonant Stokes shift," and "global Stokes shift") and some confusion regarding their meanings. The classical definition of Stokes shift is the energy difference between the maxima of the emission band and of the lowest-energy absorption (excitation) band involving the same two electronic states,[41] and is therefore taken to reflect the degree of relaxation in the excited state (i.e., the offset between the equilibrium configurational coordinates of the two states). For QDs, the closest to this definition is the so-called resonant Stokes shift $\Delta_{ST}(r)$, which is the difference between the excitation and the zero-phonon line frequencies in fluorescence line narrowed spectra,[43] and is explained on the basis of the band-edge exciton fine structure. The eightfold degeneracy of the lowest exciton state $1S_{(e)}1S_{3/2(h)}$ is partially lifted in wurtzite CdSe and CdTe QDs, yielding five levels (viz., E_0^U, $E_{\pm 1}^U$, E_0^L, $E_{\pm 1}^L$, and $E_{\pm 2}$, in order of decreasing energy).[44] $\Delta_{ST}(r)$ is taken to be the energy difference between the lowest two fine-structure states, and has been reported to increase from 2 to 20 meV for CdSe QDs in the 9–2.2 nm diameter range.[43] The nonresonant Stokes shift, $\Delta_{ST}(nr)$, is the energy difference between the lowest-energy absorption peak and the PL peak of an ensemble of QDs,[42,43] and has been reported to be larger than $\Delta_{ST}(r)$ and size dependent (20–100 meV for CdSe QDs in the 9–2.2 nm diameter range[42,43]). The discrepancy between $\Delta_{ST}(r)$ and $\Delta_{ST}(nr)$ has been attributed to the combined effects of the inhomogeneous size distribution and the exciton fine structure.[43] Most of the $1S_{(e)}1S_{3/2(h)}$ oscillator strength is carried by the upper two fine-structure exciton states and therefore $\Delta_{ST}(nr)$ is the energy difference between the mean position of the two upper states (E_0^U and $E_{\pm 1}^U$) and the mean position of the emitting state. The effect of the size distribution on $\Delta_{ST}(nr)$ is due to the fact that the absorption cross sections at energies far above the band-edge scale with the volume,[23] and therefore larger QDs will absorb relatively more light, resulting in a redshift of the ensemble PL spectrum from the statistically weighted maximum (for excitation at energies far above the band edge). For nanorods, $\Delta_{ST}(nr)$ is usually referred to as the global Stokes shift[45,46] and has been reported to increase monotonically with increasing aspect ratio (AR), reaching 100 meV for AR=10.[45] This trend has been interpreted solely in terms of the exciton fine structure. However, different values have been reported by different groups for the same AR range (e.g., 35 ± 7 meV,[46] or 50 ± 10 meV,[45] in the 2–4 AR range, for similar diameters). It is thus likely that the influence of size and shape inhomogeneities on $\Delta_{ST}(nr)$ have been overlooked for nanorods.

The $\Delta_{ST}(nr)$ values obtained in the present work for CdSe, CdTe, and type-I CSS QDs are similar and not significantly size dependent (viz., 21 ± 4 and 20 ± 8 meV, for CdSe and CdTe QDs, respectively, in the 2.5–5 nm diameter range, 22 ± 8 meV for CSS QDs, regardless of shell composition and thickness). A $\Delta_{ST}(nr)$ value of 57 meV was determined for CdSe nanorods ($L=10.5 \pm 1.5$ nm and $d=2.9 \pm 0.3$ nm). The absence of size dependence is in contrast with the reports mentioned above.[42,43] This is probably due to the fact that the $\Delta_{ST}(nr)$ values reported here were obtained from PLE and PL spectra of diluted solutions of highly efficient QDs. PLE spectra are better suited than absorption spectra to minimize the effects of size inhomogeneity since spectral resolution allows for selection of subensembles of QDs, effectively narrowing the size dispersion of the QDs probed. The use of samples with low optical densities avoids reabsorption, further minimizing the effects of size dispersion. Reabsorption and reemission will lead to larger $\Delta_{ST}(nr)$ since larger QDs in the ensemble reabsorb the emission from smaller QDs and subsequently emit at lower energies. These results show that the increase observed in Fig. 7 for the $\Delta_{ST}(nr)$ values of the CdTe/CdSe heteroNCs emitting at energies lower than 1.95 eV (i.e., in the type-II regime) is not due to increased size and/or shape inhomogeneities but rather reflect a progressive increase in the degree of relaxation in the lowest-energy exciton state.

4. Evolution of the absorption cross section

We will now analyze the μ^*_{SS} trend displayed in Fig. 7. It is clear that the μ^*_{SS} values of the CdTe/CdSe heteroNCs follow the volume-averaged trend up to the sample emitting at 1.88 eV (44% $V_{fr(\mathrm{CdSe})}$) and then decrease at a much smaller rate, remaining essentially constant in the 1.75–1.50 eV interval (i.e., for samples with $V_{fr(\mathrm{CdSe})} > \sim 50\%$ and after the onset of branching). To understand the meaning of this observation, it is important to recall that the use of the PL peak energy as a surrogate variable for the NC size will effectively normalize the trends for the (unknown) exciton volume, while still reflecting its increase or decrease, since the decrease in the confinement energies of the electron and hole will result in a shift of the exciton levels to lower energies. This point is well illustrated by the μ^*_{SS} values of the type-I CSS QDs, which follow the frequency-dependent trend of CdSe QDs (viz., CdSe/ZnSe CS QDs: PL at 2.267 eV, $\mu^*_{SS}=0.071$; CdSe/ZnSe/ZnS CSS QDs: PL at 2.24 eV; $\mu^*_{SS}=0.065$), as expected considering that both electron and hole are primarily confined to the CdSe core. The small decrease in μ^*_{SS} correlates well with the small shift of the $1S_{3/2(h)} \rightarrow 1S_{(e)}$ transition to lower energies upon shell growth, showing that the PL energy is a sensitive indicator for the effective extension of the electron and hole wave functions, and consequently also reflects the e-h wavefunction overlap integral Θ.

The fact that the μ^*_{SS} values of the CdTe/CdSe heteroNCs initially follow the volume fraction averaged trend is thus consistent with the assignment made above (Sec. IV C), and also with the temperature dependence of the PL bands in the 293–400 K range (Sec. IV B). In the type-$I^{1/2}$ regime, the electron wave function is delocalized over the whole heteroNC, thereby experiencing the volume fraction averaged properties of CdTe and CdSe (i.e., dielectric constant, thermal-expansion coefficients, electron-lattice interaction, etc.). In this regime, the PL shift to lower energies and the decrease in Θ will be correlated since they are both caused by the increasing delocalization of the electron wave function over the growing heteroNC. Deviation from the volume-averaged trend occurs near the onset of the type-II regime. It is important to notice that beyond this point, the μ^*_{SS} values decrease only slightly, despite the shift of the PL peak to lower energies and the progressive increase in the $\Delta_{ST}(nr)$ and FWHM. This implies that the total oscillator strength of the quasi-indirect transition $1S_{3/2(h)}(\mathrm{CdTe}) \rightarrow 1S_{(e)}(\mathrm{hetero})$ is preserved in the spatially indirect transition $1S_{3/2(h)}(\mathrm{CdTe}) \rightarrow 1S_{(e)}(\mathrm{CdSe})$ [or $1S_{3/2(h)}(\mathrm{CdTe}) \rightarrow 1\Sigma_{(e)}(\mathrm{CdSe})$], and is redistributed over a wider frequency range as a result of the dispersion of both the $1S_{3/2(h)}(\mathrm{CdTe})$ and the $1S_{(e)}(\mathrm{CdSe})$ [or $1\Sigma_{(e)}(\mathrm{CdSe})$] states in k space, which also results in a larger degree of relaxation and therefore larger $\Delta_{ST}(nr)$. This is analogous to the classical description of an electric dipole allowed transition between two electronic states in terms of the configurational coordinate model, where the Franck-Condon overlap factors merely redistribute the total transition moment among all possible vibronic transitions.[41]

The total interband oscillator strength f_{TOT}, obtained by integrating over all the exciton states, is determined by the total interband matrix element per unit ion pair, $|\langle \psi_{CB}|p|\psi_{VB}\rangle|$, and the number of units per QD. Since $|\langle \psi_{CB}|p|\psi_{VB}\rangle|$ is determined by the semiconductor's chemical composition and crystal lattice (i.e., by the Bloch functions), which are size independent, it can be expected that the volume normalized total oscillator strength (f_{TOT}/V) will be size independent.[23] At any size, f_{TOT} is distributed over all the exciton transitions, according to the density of states involved in each transition. The increase in Θ induces a redistribution of f_{TOT}/V so that the fraction taken by the lowest exciton state (f_{SS}/V, which determines μ_{SS}) becomes strongly size dependent, as clearly demonstrated for CdSe and CdTe QDs.[23] Figure 6 shows that μ_{SS} decreases much faster with increasing volume for CdTe/CdSe heteroNCs than for CdSe and CdTe QDs. However, the total absorption cross section per ion-pair unit (μ_{TOT} proportional to f_{TOT}/V) remains essentially constant (viz., 0.62 ± 0.05 in the 12–100 nm^3 volume range) and is very similar to that observed for CdTe and CdSe QDs (viz., 0.62 ± 0.05 and 0.63 ± 0.05, respectively, in the 2.5–7 nm diameter range). This shows that $|\langle \psi_{CB}|p|\psi_{VB}\rangle|$ remains unaffected in the CdTe/CdSe heteroNCs, as expected considering that the Bloch functions for CdTe and CdSe are quite similar.[23] These observations endorse the assignment presented above, and show that the oscillator strength per ion-pair unit (f_{SS}/V) of the lowest-energy exciton transition (quasi-indirect or indirect) of CdTe/CdSe heteroNCs is redistributed from higher-energy transitions of both the CdTe and the CdSe segments, in response to the reduction in Θ induced by the increase in $V_{fr(\mathrm{CdSe})}$.

The results above also show that the formation of a spatially indirect exciton does not necessarily lead to a substantial reduction in f_{SS} per ion-pair unit but primarily redistributes it over a wider frequency range. This redistribution may be accompanied by reduction if the electron confinement energies also decrease due to a (roughly) isotropic increase in $V_{fr(\mathrm{CdSe})}$. In the present case, however, the transition to the type-II localization regime coincides with the onset of branching. As discussed above, the growth of the CdSe segment of the heteroNC occurs then primarily in the length direction and hence does not substantially affect the electron confinement energies. The gradual increase in FWHM and $\Delta_{ST}(nr)$ reflects the progressively larger spatially indirect character of the lowest-energy exciton transition, in agreement with the model discussed above (Sec. IV C). It should be noted that the description of the spatially indirect exciton transition in terms of band offset diagrams is inadequate to explain the redistribution of f_{SS}/V and the increase in FWHM and $\Delta_{ST}(nr)$ observed in the type-II regime since the exciton dispersion in k space is neglected.

It is interesting to estimate the trend for the absorption cross section of the lowest-energy exciton transition per heteroNC (σ_{SS}) since the theoretically predicted trends[1,2] concern the oscillator strength per heteroNC (f_{SS}) rather than per ion-pair unit (f_{SS}/V). The volume dependence of σ^*_{SS} can be estimated from the μ^*_{SS} values given in Fig. 6 ($\sigma^*_{SS} \approx \mu^*_{SS} V_{\mathrm{NC}}$).[23] Two strikingly different trends are observed: σ^*_{SS} decreases proportionally to $V^{1.6}_{\mathrm{NC}}$ in type-$I^{1/2}$ regime (i.e., up to $V_{\mathrm{NC}}=19$ nm^3), and then increases linearly with increasing V_{NC} in the type-II regime. The decrease in σ^*_{SS} with increasing volume is in agreement with theoretical models

based on the effective-mass approximation[1,2] but is more pronounced than predicted (f_{SS} is proportional to Θ, which is predicted to be proportional to $V_{NC}^{1.3}$ for spherical QDs in the type-II regime[1]). This difference may be due to the anisotropic shape of the CdTe/CdSe heteroNCs investigated here, which leads to a larger degree of spatial separation than that achievable in a spherical heteroNC of comparable V_{NC}. The increase in σ_{SS}^{*} observed for the heteroNCs in the type-II regime can be ascribed to electron-hole spatial correlation, as proposed by Laheld and co-workers[1] for embedded type-II QDs in the weak confinement regime (i.e., $r_{QD} > a_0$, where a_0 is the Bohr radius of the confined carrier). In this case, the electron and hole become spatially correlated due to Coulomb interactions, and f_{SS} is predicted to increase with r_{QD}^2 ($V_{NC}^{2/3}$). The stronger than expected dependence observed here may be a consequence of the highly anisotropic character of the heteroNCs. As mentioned above, the onset of the type-II regime coincides with the onset of branching, which implies that the electron in the CdSe segment of the heteroNC will be weakly confined in the length direction, although still strongly confined in two dimensions. This may enhance the coulomb interactions and increase the e-h spatial correlation.

E. Exciton Lifetimes

1. Evolution of the room-temperature exciton lifetimes

The PL decay curves of nearly all the CdTe/CdSe heteroNC samples investigated in this work are well described by a biexponential function, implying the existence of two kinetically distinct relaxation channels. The only exceptions are the PL decay curves of samples with low QYs ($\leq$30%) or large inhomogeneities in size and shape (regardless of the PL QY), which cannot be adequately described by single-exponential or biexponential fitting functions. The multiexponential character of the PL decays of low QY samples can be ascribed to the contribution of exciton trapping, which is known to lead to complex exciton relaxation dynamics[16] while sample inhomogeneity leads to multiexponential decays due to the convolution of a large number of different decay rates. In the discussion below, only samples that yielded biexponential decays will be considered, unless otherwise stated.

It should be noted that the PL decay curves of samples 21%CdSe and 39%CdSe have been described in Ref. 15 (samples B and C, respectively) by single-exponential functions, in contrast to the analysis presented here. The reason for this discrepancy lies in the fact that the PL decay curves reported for these two samples in Ref. 15 have been measured using too high repetition rates (viz., 2.5 MHz instead of 1 MHz, as used in the present work). This resulted in insufficiently wide acquisition time windows (i.e., 400 ns), causing the slow decay component to be overlooked due to its relatively small amplitude in the decay transients of these two samples.

Single-exponential decays are usually attributed to purely radiative exciton recombination, even for samples with PL QYs lower than unity. This is based on the assumption that the ensemble consists of bright QDs (with near unity QY) and inefficient QDs (essentially dark), and therefore that the decay curves are dominated by the contribution of the efficient QDs.[47–49] The validity of this assumption has been demonstrated by a number of groups.[23,47,48] This raises the possibility that the biexponential decays observed here consist of two radiative relaxation channels. To check whether this hypothesis is valid, the PL decay curves of two efficient CdTe/CdSe heteroNC samples (39%CdSe and 92%CdSe, PL QY $\geq$ 70%) were measured at several different PL energies (Fig. 8).

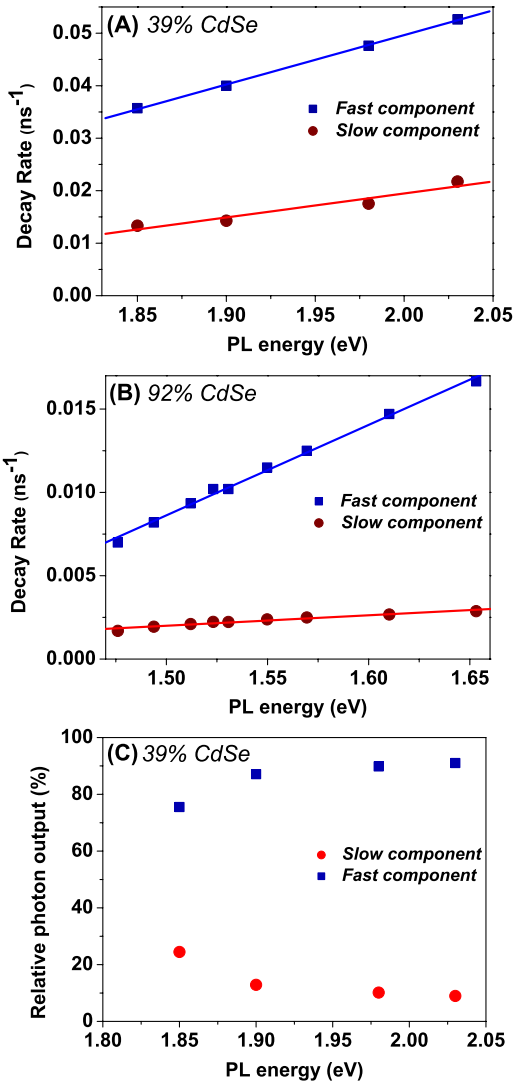

FIG. 8. (Color online) Frequency dependence of the decay rates for the fast and slow component of the PL decay curves of CdTe/CdSe heteroNCs with a 2.6 nm CdTe core and two different CdSe volume fractions: (A) 39%; and (B) 92%. The solid lines are linear fits to the data. (C) Frequency dependence of the relative photon output for the fast and slow decay channels of sample 39%CdSe.

The linear frequency dependence of the decay rates (Γ_{FAST} and Γ_{SLOW}) evidenced in Fig. 8 is in agreement with Fermi's golden rule and implies that indeed both decay channels are radiative.[23] This is consistent with the high PL QYs displayed by both samples ($\geq$70%). Further, the different slopes for the trends and the frequency dependence of the relative photon outputs of the two channels are consistent with two emitting states close in energy. These results rule

out the possibility that the fast decay rate is due to contributions of both radiative and nonradiative relaxation processes. The observation of two radiative decay rates can be interpreted either as an intrinsic property of CdTe/CdSe heteroNCs (i.e., every NC contains two emitting states close in energy) or as a consequence of ensemble inhomogeneities in size, shape, and heterointerface composition. These two possible explanations will be referred hereafter as the "intrinsic" and the "subensemble" scenarios.

Spectral resolution effectively allows the selection of subensembles of QDs (or heteroNCs), making it possible to observe single-exponential (and frequency-dependent) PL decays from inhomogeneous QD samples,[23] provided the inhomogeneity is sufficiently small (less than 10% for single composition QDs). The spontaneous emission rates extracted from such decay curves still correspond to the mean value of log-normal distributions but with a width that is sufficiently narrow to allow fundamental relationships, such as the linear dependence on the PL frequency, to be observed.[23] However, increasing the inhomogeneity of QD ensembles does not result in biexponential PL decay curves but yields instead multiexponential decays, due to the convolution of a large number of slightly different rates. As mentioned above, this is also the case for the CdTe/CdSe heteroNCs investigated here. Therefore, to explain the observation of two radiative decay rates, regardless of the monitored PL frequency (Fig. 8), the subensemble scenario requires the ensemble to consist of two distinct subpopulations of heteroNCs emitting at slightly different energies and yet with significantly different rates so that spectral overlap would occur at all PL frequencies yielding biexponential PL decays in which the amplitude of each characteristic time constant would be determined by the relative contribution of each subpopulation. Moreover, the relative contribution of these two subpopulations must be highly reproducible since the batch to batch variability in the optical properties of efficient samples is very small (viz., $\leq$10 meV for the PL peak position and $\leq$10% for the decay constants and amplitudes of both decay channels). Such a reproducible bimodal distribution is very unlikely for colloidal heteroNCs since the dispersion in size, shape, and heterointerface composition is determined by local fluctuations in the reaction conditions (viz., concentration of precursors and temperature),[3] which are stochastic in nature. Accordingly, the TEM images of the CdTe/CdSe heteroNC samples investigated in this work have indicated only variable degrees of polydispersity, ranging from $\leq$10% for samples showing biexponential PL decays to as large as 50% for samples with multiexponential PL decays. The absorption and PLE spectra (Secs. IV C and IV D above) are also not consistent with a bimodal distribution of heteroNCs. These arguments imply that the subensemble scenario is unlikely and provide support for the intrinsic scenario.

To further elucidate which scenario is more plausible, the evolution of the two decay rates with increasing $V_{fr(\mathrm{CdSe})}$ was analyzed in detail. The decay rates and the relative photon outputs for the two recombination channels of all the CdTe/CdSe heteroNC samples are presented as a function of the PL peak energy in Fig. 9. The nature of the fast decay channel changes over the growth of the heteroNCs. For the initial samples, with $V_{fr(\mathrm{CdSe})} < \sim 5\%$, the QY is lower ($\leq$30%) and

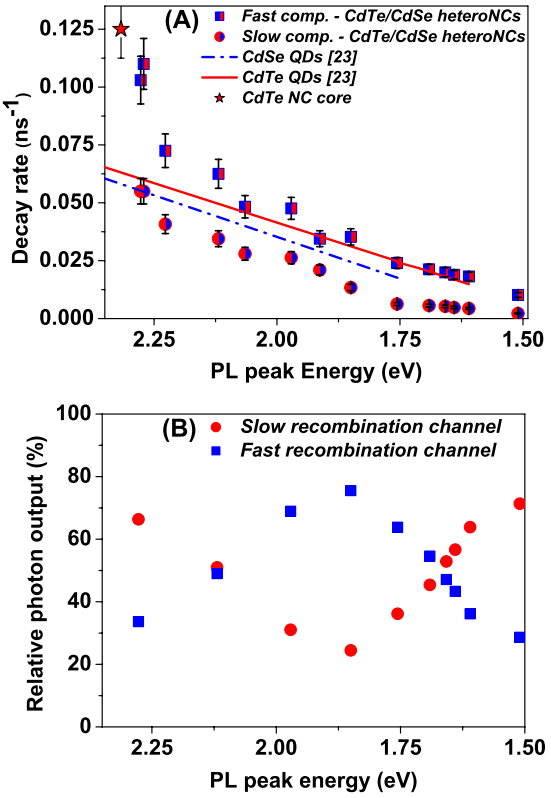

FIG. 9. (Color online) (A) Decay rates for the fast and slow component of the PL decay curves of CdTe/CdSe heteroNCs with a 2.6 nm CdTe core and increasing CdSe volume fraction, as a function of the PL peak energy. The lines give the trends for the radiative decay rates of CdSe and CdTe QDs reported in the literature (Ref. 23). (B) Relative photon output for the fast and slow decay channels as a function of the PL peak energy for the same samples shown in (A).

the photon output is dominated by the slow decay channel. This implies that the fast decay channel for the initial samples also contains nonradiative contributions. As the growth of the CdSe part proceeds, the QYs increase and the decay curves become truly biexponential (as judged from the fit quality), indicating that both channels are primarily radiative for samples emitting below ~2.2 eV ($V_{fr(\mathrm{CdSe})} \geq 21\%$). The relative photon output of the fast channel then progressively increases up to the onset of the transition from type-I$^{1/2}$ to type-II behavior (at 1.75 eV), when the relative photon output of the slow channel starts to increase. Concomitantly, both Γ_{FAST} and Γ_{SLOW} become slower with decreasing PL energies (i.e., increasing $V_{fr(\mathrm{CdSe})}$). This can be ascribed to the decrease in the e-h overlap Θ due to the progressive localization of the electron wave function in the CdSe part of the heteroNC. An explanation for the difference between Γ_{FAST} and Γ_{SLOW} will be presented below (Secs. IV E 2 and IV E 4).

The fast decay rate decreases rapidly up to ~2.2 eV, and then follows a frequency dependence that is very similar to that of CdTe QDs. Γ_{SLOW} is much slower than Γ_{RAD} of both CdTe and CdSe QDs at all PL energies, and follows a roughly linear frequency dependence that becomes less pronounced for PL energies lower than 1.75 eV. Apart from the

small change in the slope of the frequency dependence of Γ_{SLOW}, the transition from the type-$I^{1/2}$ to the type-II regime does not lead to pronounced changes in the decay rate trends, which is consistent with a gradual increase in the spatially indirect character of the exciton, as discussed above. The fact that Γ_{FAST} follows the same frequency dependence as Γ_{RAD} of CdTe QDs does not imply that the fast decay channel is due to the radiative recombination of a "CdTe-like" direct exciton. Γ_{FAST} of a CdTe/CdSe heteroNC is the same as Γ_{RAD} of a CdTe QD emitting at the same frequency but is much slower than that of a similarly sized CdTe QD. For example, a CdTe/CdSe heteroNC emitting at 1.75 eV has a volume of 20 nm^3 and Γ_{FAST}=0.029 ns^{-1} whereas a CdTe QD with a similar volume (3.4 nm diameter) emits at higher energies (2.136 eV) with faster Γ_{RAD} (viz., 0.051 ns^{-1}).[23] In contrast, type-I CSS QDs also follow the frequency-dependent trend of the exciton lifetimes of the core materials but show a faster radiative decay rate than a similarly sized single-component QD (e.g., CdSe/CdS/ZnS CSS QDs and CdSe QDs emitting at 2.056 eV show a very similar Γ_{RAD}, viz., 0.0365 ns^{-1} and 0.038 ns^{-1}, respectively, but have very different sizes: 10 nm and 4.5 nm, respectively).

The linear frequency dependence observed for the spontaneous emission rates Γ_{RAD} of CdSe and CdTe QDs has been shown to result from a cancellation between two different effects (viz., increasing QD volume leads to both an increase in the total transition dipole moment P per QD and a decrease in the overlap integral Θ).[23] The observation that Γ_{RAD} of CdTe QDs and Γ_{FAST} of CdTe/CdSe heteroNCs are similar at the same transition frequency ω_{SS} shows that the oscillator strength f_{SS} per NC is the same in both cases (Γ is proportional to f_{SS}). This implies that the product ΘP^2 [see Eq. (3) above] is comparable for the two cases. The similarity observed between the frequency dependences can thus be interpreted as a consequence of the partial normalization introduced by using the PL peak energy as variable.

From the discussion above it follows that the two decay rates can be ascribed to two exciton states with different degrees of electron-hole spatial separation. The well-defined and reproducible trends observed in Fig. 9 for both Γ_{FAST} and Γ_{SLOW} are consistent with the evolution of intrinsic heteroNC properties with increasing $V_{fr(CdSe)}$ but are hard to explain within the subensemble scenario since that would require the two subpopulations of heteroNCs to evolve in a deterministic manner. This and the arguments presented above support the intrinsic scenario as the most likely explanation for the observation of two radiative decay rates. However, a distinct feature of this scenario is that it implies the kinetic isolation of the two emitting states and the absence of thermalization between them at room temperature since equilibration would lead to the observation of only one Γ_{RAD}. This requires not only a slow transition rate from the lower to the upper state (to prevent equilibration) but also a slow relaxation from the upper to the lower state since a fast relaxation would lead to depletion of the upper-state population and, consequently, to only one radiative decay rate. It is thus clear that the investigation of the temperature dependence of the optical properties may help to unambiguously identify the origin of the two PL channels.

2. *Temperature dependence of the PL spectra and PL decay in the 4.2 to 300 K range*

The temperature (T) dependence of the PL spectra and decay curves of a representative CdTe/CdSe heteroNC sample (viz., 39%CdSe) has been investigated in the 4.2–300 K range. This sample is ideally suited for this study. First, it exhibits very well-defined frequency-dependent trends for both decay channels (Fig. 8). Second, it is in the type-$I^{1/2}$ localization regime, which implies relatively narrow bandwidths (Fig. 7). Finally, it has a narrow size distribution (10%) and a very high PL QY (80%, temperature independent in the 4.2–380 K range).

We will restrict our analysis to the aspects relevant to establishing which of the two scenarios most adequately explains the observed behavior. A detailed investigation of the T dependence of the exciton lifetimes and PL spectra of CdTe/CdSe heteroNCs is beyond the scope of this paper and will be reported elsewhere. The PL decay curves are strongly dependent on both the temperature and the PL frequency (Fig. 10). The overall frequency dependence of both Γ_{FAST} and Γ_{SLOW} remains similar to that observed at room temperature, although both decay rates become slower with decreasing T's (e.g., 80 ns and 1.1 μs, respectively, at 4.2 K). A close examination of the decay curves obtained while monitoring the lower-energy PL reveals a very interesting feature: a strongly T-dependent rise time, which increases from 3 ns at 250 K to 20 ns at 20 K and to 120 ns at 4.2 K [Figs. 10(B)–10(D)]. In contrast, the decay curves acquired while monitoring the higher-energy side of the PL band do not show a rise time but instead display faster decays at early times [Figs. 10(B) and 10(D)].

This behavior is strongly reminiscent of that previously reported for CdTe QD solids,[50] which has been attributed to energy transfer (ET) from smaller to larger QDs in the ensemble. However, in the present case, very diluted solutions (viz., $\leq$0.1 μM, optical densities at 3.1 eV $\leq$0.2) are investigated, and consequently inter-NC ET can be ruled out since ET is strongly distance dependent ($1/d^6$-$1/d^4$).[51] Therefore, the rise time observed in the decay curves of the lower-energy PL accompanied by a fast decay at early times in the transients of the higher-energy PL indicates intraheteroNC ET, i.e., energy relaxation between two different exciton states of a CdTe/CdSe heteroNC. The strong T dependence of the rise time implies that this relaxation is phonon assisted. We note that this observation is incompatible with the subensemble scenario and provides unambiguous evidence in favor of the intrinsic scenario. Nevertheless, the rise times above 250 K seem to be sufficiently fast to guarantee thermalization between the two states, in contrast with the observation of two radiative decay rates at room temperature. A possible explanation for this discrepancy can be found in the T dependence of the PL spectra.

The decrease in T also induces remarkable changes in the PL spectra [Fig. 10(A)]. The most relevant for our purposes is the change in the spectral shape since it clearly demonstrates that the PL spectra consist of (at least) two bands. For example, the PL spectrum at 4.2 K consists of a stronger peak at 2.025 eV (FWHM=70 meV), accounting for 70% of the emitted photons, and a weaker peak at 1.90 eV

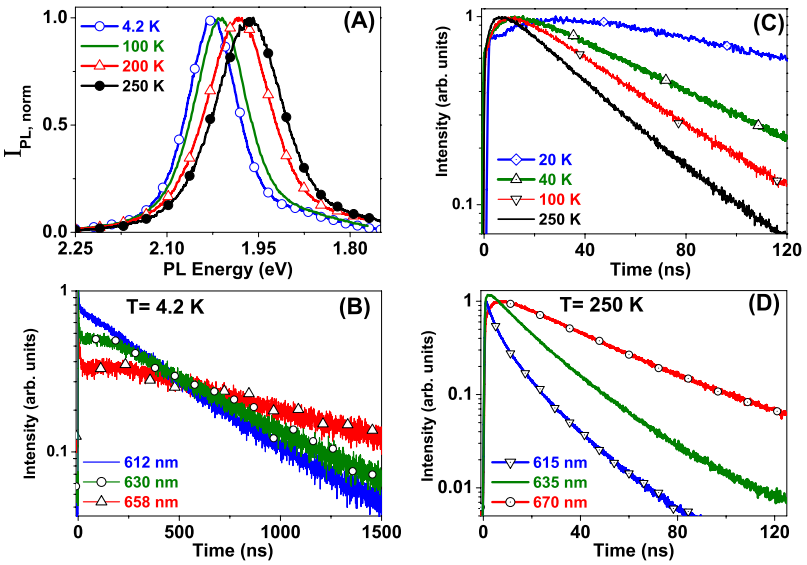

FIG. 10. (Color online) Normalized temperature dependent PL spectra (A) and decay curves [(B)–(D)] of CdTe/CdSe heteroNCs consisting of a 2.6 nm CdTe core and 39% CdSe volume fraction (sample 39%CdSe), measured at the temperatures indicated. The PL decay curves shown in (B) and (D) were obtained at three different emission wavelengths (PL peak and ~20–30 nm redshifted and blueshifted). The decay curves presented in (C) were all measured at the lower-energy side of the PL emission band (approximately 50 meV from the PL peak). To facilitate the observation of the rise times, only the initial part of the decay curves is shown (the full acquisition time window ranges from 5000 ns at 4.2 K to 1000 ns at 300 K).

(FWHM=200 meV). Increasing temperatures will affect the spectral position and bandwidth of both peaks, but not in the same way. The FWHM of the higher-energy band increases continuously from 70 to 120 meV in the 4.2–300 K range while that of the lower-energy band remains constant at 205 ± 20 meV up to 250 K and then drops to 145 meV at RT. The increase in the linewidth of PL peaks with increasing temperature is typically ascribed to the increase in the homogeneous broadening, as a result of enhanced dephasing due to exciton-phonon scattering.[26,42,52] This model explains well the trend for the higher-energy band but is unable to account for the atypical behavior exhibited by the lower-energy band.

The T dependence of the band positions is also remarkable. The spectral shift is essentially the same for both bands up to 250 K (~70 meV redshift) but becomes dramatically different at higher T's: the lower-energy peak undergoes an even faster bathochromic shift (80 meV from 250 to 300 K) while the higher-energy band displays a 20 meV blueshift. Temperature-dependent spectral shifts are usually ascribed to the T dependence of the band gap,[15,26,52] which is nevertheless not yet well understood for semiconductor NCs.[52] Although the T dependence of the band gap of CdSe and CdTe QDs has not yet been studied in detail, it is clear that the redshifts observed here for the lower-energy peak are much larger (a factor 3–5) than those expected for CdTe or CdSe QDs of similar sizes.[15] Moreover, the blueshift observed for the higher-energy peak upon increasing T above 250 K is unprecedented for CdTe or CdSe based NCs. It is also interesting to notice that the FWHM and peak position of the higher-energy PL peak at RT are comparable with the FWHM and peak position of the lowest-energy absorption peak (see Fig. 7 above), suggesting that the same levels are involved in the two transitions. In contrast, the lower-energy PL peak has no equivalent in the absorption or PLE spectra, indicating a small absorption oscillator strength, which is consistent with the longer lifetimes exhibited by the lower-energy PL. These observations provide further support for the intrinsic scenario.

The complex T dependence observed here for the PL spectra of CdTe/CdSe heteroNCs is probably due to an intricate interplay between the CdSe and CdTe components, and may also be influenced by reconstructions induced by phase transitions in the surfactant layer, as previously observed for organically capped CdSe and CdTe colloidal QDs.[24,26,53] Although a comprehensive analysis of these intriguing observations lies beyond the scope of the present work, the results above undoubtedly demonstrate that the population and position of the energy levels, as well as the relative offset between them, are continuously changing as a function of the temperature, and undergo a dramatic change just below RT. Therefore, we propose that at RT the offset between the two emitting states is such that the upper to lower relaxation primarily occurs via tunneling, and the lower to upper transition rate becomes negligible (see Fig. 11 for an schematic energy-level diagram). We note that this is analogous to the singlet to triplet intersystem crossing in organic molecules,

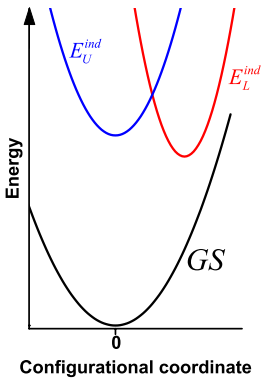

FIG. 11. (Color online). Schematic configurational coordinate diagram showing the two emitting exciton states of CdTe/CdSe heteroNCs. For simplicity the energy dispersion is taken to be parabolic for all three states but with different dispersion relations due to the different nature of each state. The offsets in energy and configurational coordinates have been chosen such that coexistence of two radiative decay channels is possible, and direct crossing to the ground state is prevented. It should be noted that the diagram is generic and only qualitatively correct. A detailed discussion regarding the nature of each state and their evolution with increasing CdSe volume fraction is presented in the main text.

for which thermalization also does not occur, but is atypical for semiconductor NCs. Indeed, a behavior similar to that observed here has never been reported for diluted solutions of single-component and type-I core/shell QDs and nanorods, despite the fact that the T dependence of the exciton lifetimes has been extensively investigated for a number of compositions [viz., CdSe QDs,[26,54] CdSe/ZnSe CS QDs,[26] CdSe/ZnSe/ZnS CSS QDs,[26] CdTe QDs,[54] CdSe nanorods,[55] PbSe QDs,[54] and InAs QDs (Ref. 54)]. This suggests that this behavior is intrinsic to CdTe/CdSe colloidal heteroNCs.

In this context, it is noteworthy that two bands have also been observed in the RT PL spectra of CdSe/CdTe heteronanorods (diameter: 4–5 nm; length 15–20 nm),[16,56] and tentatively assigned to a charge-transfer (CT) state (i.e., an indirect exciton), and to the lowest exciton state of the CdTe segment, which was presumed to be populated by back electron transfer from the long-lived CT state.[16] Although the data analysis was complicated by the multiexponential character of the PL decay curves, Jones *et al.* were able to estimate decay rates for the two emitting states by using a stochastic model in which trapping rates were also accounted for.[16] Interestingly, the decay rates estimated for the higher-energy emission (viz., 0.02–0089 ns^{-1}, depending on the sample[16]) are comparable to the Γ_{FAST} values observed in Fig. 9 while those obtained for the longer-lived PL (viz., 0.0026–0.0014 ns^{-1})[16] are similar to the Γ_{SLOW} values reported here (Fig. 9). Further, it is quite remarkable that the Γ_{FAST} values observed in Fig. 9 are also similar to the radiative decay rates reported by Oron *et al.*[19] for concentric CdTe/CdSe core/shell heteroNCs (viz., from 0.05 ns^{-1} for 3.9 nm cores to 0.007 ns^{-1} for a core/shell with a 2.5 nm shell).

This suggests that the observation of two emitting states in the present work is related to the shape of the CdTe/CdSe heteroNCs investigated here, which share aspects of both concentric core/shell QDs (viz., spherical CdTe core surrounded by CdSe) and heteronanorods (viz, the CdSe part of the heteroNC grows anisotropically, gradually forming branches). This could lead to the coexistence of two indirect exciton states, denoted as E_U^{ind} and E_L^{ind} in Fig. 11 (upper and lower states, respectively). These two states should be present in all samples investigated here, albeit with different relative contributions, given that shape anisotropy is manifested since the beginning of the CdSe overgrowth (heteroNCs with $V_{fr(\mathrm{CdSe})}$ as small as 1% are already prolate). Nevertheless, clear evidence for the presence of two emitting states is only observed for CdTe/CdSe heteroNC samples with $V_{fr(\mathrm{CdSe})} \geq 21\%$ (Sec. IV E 1). As discussed above, samples with lower $V_{fr(\mathrm{CdSe})}$ have low PL QYs ($\leq 30\%$) and therefore exhibit multiexponential decay curves due to the contribution of nonradiative decay channels. It should be pointed out that our results clearly show that the higher-energy PL cannot be ascribed to "backtransfer" to the CdTe component, as suggested in Ref. 16 since this would result in emission at 2.32 eV. Before discussing the possible nature of these two states and the reasons for their different properties, it is useful to briefly consider the exciton fine structure and exciton relaxation in CdSe and CdTe QDs.

3. Fine-structure exciton states and exciton relaxation

In the framework of the effective-mass approximation, the lowest exciton state (viz., $1S_{(e)}1S_{3/2(h)}$) of spherical CdSe and CdTe NCs with cubic lattice structure (zinc blende) is eightfold degenerate.[34,44] The lowest electron state ($1S_{(e)}$) is doubly degenerate with respect to its spin projection whereas the lowest hole state ($1S_{3/2(h)}$) is fourfold degenerate with respect to the projection of its total angular momentum. The lowest exciton state in nanorods has a different symmetry and hole angular momentum (viz., $1\Sigma_{(e)}1\Sigma_{1/2(h)}$) but is also degenerate (fourfold).[35] The combined effects of crystal-field asymmetry, shape anisotropy, and electron-hole exchange interaction partially lift the degeneracy of the exciton states.[35,44,55] The splitting and the transition oscillator strengths of the fine-structure states, as well as their order, is very sensitive to the NC size and shape.[35,44,55] For example, as mentioned above, five levels are obtained for spherical CdSe and CdTe NCs with the wurtzite crystal structure or for prolate CdTe NCs with the zinc-blende crystal structure.[44] Two of these states are optically passive in the electric dipole (ED) approximation, and are therefore usually referred to as dark states.[44]

The intraband and interband relaxation in CdSe QDs has been investigated in detail and is well understood.[26,54,57,58] Relaxation from the higher exciton states ($1P$, $1D$, etc.) to the lowest exciton state ($1S_{(e)}1S_{3/2(h)}$) is very fast (viz., 300–500 fs),[57,58] in contradiction with the slower rates predicted on the basis of the phonon bottleneck effect (i.e., phonon energies available in NCs would be too small to efficiently bridge the energy gap between the quantum-confined exciton levels). This fast intraband relaxation has been shown to occur via an Auger-type mechanism in which efficient energy transfer from electron to hole occurs followed by fast hole relaxation.[58] The final and slowest (viz., 700–1000 fs) intraband relaxation step occurs within the five exciton fine-structure states of the $1S_{(e)}1S_{3/2(h)}$,[57] and populates the close-lying $E_{\pm 1}^L$ and $E_{\pm 2}$ exciton levels (i.e., the "bright" and "dark" excitons, respectively[44]), from which emission takes place. The equilibrium between these two states determines the T dependence of the exciton lifetimes.[26,54,55] The thermalization between the $E_{\pm 1}^L$ and $E_{\pm 2}$ exciton levels requires a spin flip and takes 230–430 fs at 300 K.[57]

4. Nature of the two emitting states

From the points above it can be concluded that the electron-hole interaction has a significant impact on the optical properties of CdSe and CdTe QDs since it plays a decisive role both in determining the exciton relaxation rates and in partially lifting the exciton degeneracy. The weaker e-h interaction induced by the (partial) spatial separation can be thus expected to affect the energy-level structure and relaxation of indirect excitons in CdTe/CdSe heteroNCs. Indeed, slower Auger relaxation rates have been reported for CdTe/CdSe core/shell QDs.[19] Moreover, the electron-spin relaxation rates in CdSe/CdTe heteronanorods have been shown to be one order of magnitude slower than those observed in CdSe nanorods, consistent with a weaker e-h exchange interaction.[56] Therefore, the observation below 250 K of a slow and phonon-assisted relaxation between the upper and lower emitting states of CdTe/CdSe heteroNCs (Fig. 10) can be understood as a consequence of the weaker e-h coupling. The exciton relaxation within the fine-structure levels

would then occur to a greater extent by phonon-assisted pathways, and phonon bottleneck effects could become evident, explaining the strong T dependence observed for the rise times. Relaxation processes requiring a "spin flip," such as the $E^L_{\pm 1} \rightarrow E_{\pm 2}$,[54–57] should also become slower due to the weaker e-h exchange interaction. It should be noted that the increase in the decay times with decreasing T implies that the lowest-energy levels have longer lifetimes, either due to their spin projections or a more pronounced e-h spatial separation or a combination of both.

As mentioned above, the observation of two radiative decay rates at RT requires the lack of thermalization between the two emitting states, which can be qualitatively explained by an energy-level diagram similar to the one shown in Fig. 11. This diagram implies a significant energy barrier for the $E^{ind}_U \rightarrow E^{ind}_L$ crossing and a large degree of relaxation in the lower state E^{ind}_L. These requirements can be satisfied by two exciton states with different degrees of localization of the electron wave function in the CdSe part of the heteroNC. Considering that the observation of the two emitting states seems to require anisotropic CdTe/CdSe heteroNCs, it is possible that the states also differ regarding the total angular momentum projection along the NC long axis and the symmetry of the electron wave function (i.e., S-like or Σ-like for E^{ind}_U or E^{ind}_L, respectively). The faster radiative decay rates of the upper state E^{ind}_U (Γ_{FAST}) can be thus interpreted as evidence of a larger e-h wave-function overlap Θ whereas the slower radiative decay rates of the E^{ind}_L state (Γ_{SLOW}) can be ascribed to a combination of a smaller Θ and an ED-forbidden change in the total angular momentum. The slow $E^{ind}_U \rightarrow E^{ind}_L$ relaxation can be qualitatively understood as a consequence of the requirement of a spin flip (slower due to the weaker e-h coupling) and further diffusion of the electron wave function into the CdSe segment (which results in a relatively large energy relaxation). We note that this model also qualitatively explains the differences in the linewidths of the two states, and is consistent with the evolution of the optical properties observed upon increasing $V_{fr(\mathrm{CdSe})}$ (see Secs. IV C, IV D, and IV E 1 above). Nevertheless, it must be kept in mind that the model sketched here is too simple to accurately explain all the observations reported in the present work, and is intended only to provide a qualitative and preliminary picture, which should serve as basis for future work.

For CdTe/CdSe heteroNCs in the type-I$^{1/2}$ localization regime (such as the sample used for the T-dependent investigations described above, 39%CdSe) the upper state E^{ind}_U can be ascribed to the $1S_{3/2(h)}$(CdTe)$1S_{(e)}$(hetero) exciton state while E^{ind}_L will be the $1S_{3/2(h)}$(CdTe)$1S_{(e)}$(CdSe) indirect exciton state. This explains the different linewidths and T dependences observed for the two PL bands since emission from E^{ind}_U would be essentially the reverse of the lowest-energy absorption transition, which, as discussed above (Sec. IV C), is spatially direct (and therefore also direct in k space). In contrast, emission from E^{ind}_L requires a spatially indirect transition, which leads to broader linewidths (see Sec. IV C above). The increase in the relative contribution of the slow decay channel with increasing $V_{fr(\mathrm{CdSe})}$ (Fig. 9) can then be qualitatively understood as a consequence of the shift of the $1S_{3/2(h)}$(CdTe)$1S_{(e)}$(CdSe) exciton to lower energies, which lowers the energy barrier for the $E^{ind}_U \rightarrow E^{ind}_L$ crossing and increases the degree of relaxation in the lower state E^{ind}_L, and may also affect the feeding rates of the E^{ind}_U and E^{ind}_L states by higher exciton states.

The nature of the two emitting states for CdTe/CdSe heteroNCs in the type-II localization regime may still be same as that in the type-I$^{1/2}$ regime [i.e., E^{ind}_U and E^{ind}_L correspond to $1S_{3/2(h)}$(CdTe)$1S_{(e)}$(hetero) and $1S_{3/2(h)}$(CdTe)$1\Sigma_{(e)}$(CdSe), respectively] but it is also possible that two different indirect exciton states are involved. The lowest-energy exciton state in CdTe/CdSe heteroNCs [$1S_{3/2(h)}$(CdTe)$1S_{(e)}$(CdSe), $1S_{3/2(h)}$(CdTe)$1\Sigma_{(e)}$(CdSe), or $1S_{3/2(h)}$(CdTe)$1S_{(e)}$(hetero)], is eightfold degenerate, and therefore fine-structure levels are also expected. Despite the weaker e-h exchange interaction, large splittings may occur as a result of the enhanced (and anisotropic) internal electric field induced by the large dipole moment of the indirect exciton state.[2] We suggest that shape anisotropy may partially lift the degeneracy of the indirect exciton state giving rise to fine-structure states. The E^{ind}_U and E^{ind}_L emitting states in type-II CdTe/CdSe heteroNCs could then be two of such states, differing in terms of the extension of the electron wave function in the CdSe part of the heteroNC, in the total angular momentum projection along the NC long axis and/or the symmetry of the electron wave function (i.e., S-like or Σ-like). It is worth noting that calculations performed by Efros and co-workers have shown that even small deviations from spherical symmetry (e.g., an aspect ratio of 1.28) already suffice to partially lift the $1S_{(e)}1S_{3/2(h)}$ exciton degeneracy in CdTe and CdSe QDs.[44] Therefore, given that the shape of all CdTe/CdSe heteroNCs investigated in this work is anisotropic, the splitting of the lowest-energy indirect exciton state should be present in all samples, although to different extents depending on the CdSe volume fraction and the exact heteroNC shape. This splitting may be especially evident in the T dependence of the exciton lifetimes and PL spectra. However, further work is needed to reliably establish the extent to which the optical properties of CdTe/CdSe heteroNCs are affected by shape effects on the indirect (or quasi-indirect) exciton fine structure.

The energy-level structure of heteroNCs may also be affected by quantum-mechanical coupling between different states.[4,59,60] From this perspective, the CdTe/CdSe colloidal heteroNCs investigated here can also be described as "QD molecules," consisting of a central CdTe QD bound to two (or more) CdSe QDs or Qrods (see cartoon representations in Fig. 1). Splitting of the $1S$ state in QD molecules has been experimentally observed for coupled pairs of InAs (or GaInAs) embedded QDs separated by a GaAs spacer layer.[59,60] The splitting was reported to increase with decreasing distance between the QDs, reaching 40 meV for QD pairs separated by 4 nm,[59] and also to be strongly affected by static electric fields.[60] It is also interesting to notice that the calculations recently carried out by Zunger and co-workers[4] for the electronic states of CdTe/CdSe/CdTe nanodumbbells (QD/Qrod/QD) (see Sec. III above) have shown that the character of the lowest-energy electron states depends strongly on the relative dimensions of the nanodumbbell components. In the case of a narrow CdSe rod, the lowest two states correspond to bonding and antibonding combinations of the $1S_e$ states of the two CdTe QDs while the state

immediately above them is localized in the CdSe wire.[4] In the opposite case of a wide rod, the lowest three electron states are primarily localized in the CdSe component and have an *s*-like, p_x-like, and p_z-like character, respectively.[4] Interestingly, the case of an intermediate diameter CdSe Qrod leads to a more intricate behavior due to coupling between QRod and QDs states. In this case, the lowest-energy electron state results from the bonding combination between the $1S_e$ states of the three components and is delocalized over the whole nanodumbbell while the state immediately above it corresponds to the antibonding combination of the $1S_e$ states of the two CdTe QDs, and is therefore localized on the QDs.[4] From the discussion above it follows that the nature of the emitting states in CdTe/CdSe heteroNCs is probably quite complex. However, further theoretical and experimental work is required before an unambiguous and definitive assignment can be made.

F. Comparison between the trends for PL decay rates and absorption cross sections

It is valuable to compare the trends observed for the PL decay rates and for the absorption cross sections of the lowest-energy exciton transition since the emission transition is in first approximation the reverse of the lowest-energy absorption transition. The Γ_{RAD} values are determined by f_{SS} per heteroNC, and therefore they should be compared to the σ_{SS} values. The trends observed for σ_{SS}^* and Γ_{RAD} are remarkably different. Both Γ_{FAST} and Γ_{SLOW} decrease approximately linearly with the PL frequency E_{SS}, albeit with a less pronounced dependence beyond 1.75 eV for Γ_{SLOW} (Fig. 9). This is in line with experimental results on single composition QDs (e.g., CdSe and CdTe QDs, Ref. 23) and implies that the product ΘP^2 [see Eq. (3) above] is constant so that only the dependence on ω_{SS} is manifested (Θ is the electron-hole wave-function overlap, P gives the total transition dipole moment and increases linearly with V_{NC}). In contrast, the frequency dependence of σ_{SS}^* consists of two opposite trends (reflecting the different volume dependences discussed above, Sec. IV D 4). In the type-$\mathrm{I}^{1/2}$ regime σ_{SS}^* decreases with decreasing E_{SS} in an approximately linear fashion (the decrease is supralinear for $E_{SS} > \sim 2.05$ eV and sublinear for $E_{SS} < \sim 2.05$ eV) whereas in the type-II regime, the σ_{SS}^* values strongly increase with decreasing E_{SS} (i.e., increasing $V_{fr(\mathrm{CdSe})}$ and V_{NC}). These different trends can be rationalized in terms of the product $\Theta P^2 \omega_{SS}$. In the type-$\mathrm{I}^{1/2}$ regime, the increase in P is small due to the relatively small increase in V_{NC} and is counteracted by the concomitant decrease in Θ so that the trend is essentially determined by ω_{SS}. In the type-II regime, the large increase in V_{NC} is accompanied by a relatively smaller PL shift (Fig. 3) and probably also a less pronounced Θ reduction due to the spatial e-h correlation. Consequently, the P^2 contribution dominates over $\Theta \omega_{SS}$. A discrepancy between the frequency dependences of σ_{SS}^* and Γ_{RAD} has also been observed for CdTe and CdSe QDs (Ref. 23) and was attributed to a combination of factors. First, the absorption transition is stimulated whereas the emission transition is spontaneous.[23] Further, all exciton fine-structure states contribute to the absorption cross section while the emission transition involves only the lowest state(s) (e.g., the E_U^{ind} and E_L^{ind} states in the present case). The different trends observed for the σ_{SS}^* and Γ_{RAD} values of the CdTe/CdSe heteroNCs investigated in this work are thus consistent with the assignment made above that the two emitting states are fine-structure states of the spatially indirect exciton, which implies that they carry only a fraction of the total f_{SS}.

V. CONCLUSIONS

The results presented above provide fundamental insights into the evolution of the optical properties of nanoscale spatially indirect excitons as a function of the size, shape, and composition of the heteroNC, using CdTe/CdSe as a model system. It is demonstrated that the hole wave function remains confined to the CdTe core, even for very small CdSe volume fractions ($V_{fr(\mathrm{CdSe})}$). The evolution of the optical properties of the heteroNC with the growth of the CdSe segment is thus determined by the localization regime of the electron wave function. Initially, for $V_{fr(\mathrm{CdSe})} < \sim 50\%$, the lowest-energy electron state [$1S_e$(hetero)] is delocalized over the whole heteroNC (*type-*$I^{1/2}$ regime), giving rise to well-defined and distinct absorption features. The loss in electron confinement energy is reflected in the progressive redshift of all transitions. As the growth of the CdSe segment proceeds, the $1S_e$(CdSe) state progressively shifts to lower energies, until the spatially indirect exciton transition becomes the lowest-energy absorption transition. This marks the onset of the type-II regime and is characterized by the loss of structure of the lowest-energy absorption band, accompanied by a simultaneous increase in line widths and Stokes-shift values. This can be understood by considering the dispersion in k space of the states involved in the spatially indirect exciton transition.

The energy-integrated absorption cross section per ion-pair unit of the lowest-energy exciton transition (μ_{SS}) decreases rapidly with increasing $V_{fr(\mathrm{CdSe})}$ in the type-$\mathrm{I}^{1/2}$ regime, due to the reduction in the e-h wave-function overlap integral Θ. However, μ_{SS} decreases only slightly in the type-II regime. This demonstrates that the formation of a spatially indirect exciton does not necessarily lead to a substantial reduction in the oscillator strength per ion-pair unit of the lowest-energy transition (f_{SS}/V) but primarily redistributes it over a wider frequency range. This redistribution may be accompanied by reduction, if the electron (or hole) confinement energies decrease as a result of the growth of the second component of the heteroNC. The total absorption cross section per ion-pair unit (i.e., integrating over all the exciton transitions) remains essentially constant during the growth of the heteroNC. This demonstrates that f_{SS}/V is redistributed from higher-energy transitions of both the CdTe and the CdSe segments, in response to the reduction in Θ. The energy-integrated absorption cross section per heteroNC of the lowest-energy exciton transition decreases in the type-$\mathrm{I}^{1/2}$ regime but increases linearly with the NC volume in the type-II regime, implying that the electron and hole are spatially correlated due to Coulomb interactions.

The PL decay curves of the CdTe/CdSe heteroNCs investigated in this work are well described by a combination of

two radiative decay rates, which are ascribed to two exciton states with different degrees of localization of the electron wave function in the CdSe part of the heteroNC (an upper state with a faster decay rate and a lower state with a slower decay rate). Both the fast and the slow decay rates decrease with increasing $V_{fr(\mathrm{CdSe})}$, showing a nearly linear dependence with the PL frequency. This is in contrast with the trends exhibited by the absorption cross sections (per ion-pair unit and per heteroNC) of the lowest-energy exciton transition, and implies that the two emitting states carry only a fraction of the total oscillator strength of the transition. The results presented here provide fundamental insights into nanoscale spatially indirect exciton transitions, highlighting the crucial role of a number of parameters (viz., electron-hole spatial correlation, exciton dispersion and exciton degeneracy, shape anisotropy, and electronic coupling). This knowledge should have an impact on the design of colloidal heteroNCs for optoelectronic applications and also contribute toward the development of more comprehensive theoretical models for nanoscale indirect excitons.

This work also raises a number of interesting issues that merit further investigation. First, the exact nature of the emitting states and the detailed exciton fine-structure are as yet unclear. Further, the extent to which selection rules are operative also remains to be elucidated. The impact of shape anisotropy and coupling between different exciton states on the exciton energy-level structure also needs further investigation. The exciton radiative lifetimes of colloidal QDs at low temperatures (viz., below 20 K) have been shown to be largely determined by coupling to a confined acoustic phonon.[54] It would thus be interesting to investigate the strength of the exciton-phonon coupling in CdTe/CdSe heteroNCs and its impact on the indirect exciton relaxation. Future work on the size, shape, and temperature dependence of the exciton lifetimes in CdTe/CdSe heteroNCs may shed more light on these issues.

ACKNOWLEDGMENTS

The author is indebted to Andries Meijerink, Daniël Vanmaekelbergh, and Esther Groeneveld (Utrecht University—UU) for stimulating discussions. Patrick T. K. Chin (NKI, Amsterdam) and Evelien M. van Schrojenstein Lantman (UU) are thanked for kindly supplying some of the samples investigated in this study. Financial support from the division of Chemical Sciences (CW) of the Netherlands Organization for Scientific Research (NWO) (TOP-Grant No. 700.53.308) is gratefully acknowledged.

*Corresponding author. FAX: +31-30-2532403; c.demello-donega@uu.nl

[1] U. E. H. Laheld, F. B. Pedersen, and P. C. Hemmer, Phys. Rev. B **52**, 2697 (1995).
[2] S. A. Ivanov, A. Piryatinski, J. Nanda, S. Tretiak, K. R. Zavadil, W. O. Wallace, D. Werder, and V. I. Klimov, J. Am. Chem. Soc. **129**, 11708 (2007).
[3] C. de Mello Donegá, P. Liljeroth, and D. Vanmaekelbergh, Small **1**, 1152 (2005).
[4] A. Franceschetti, L. W. Wang, G. Bester, and A. Zunger, Nano Lett. **6**, 1069 (2006).
[5] Y. Zhang, L. W. Wang, and A. Mascarenhas, Nano Lett. **7**, 1264 (2007).
[6] A. G. Winbow, A. T. Hammack, L. V. Butov, and A. C. Gossard, Nano Lett. **7**, 1349 (2007).
[7] I. R. Sellers, V. R. Whiteside, I. L. Kuskovsky, A. O. Govorov, and B. D. McCombe, Phys. Rev. Lett. **100**, 136405 (2008).
[8] A. Rogalski, Opto-Electron. Rev. **16**, 458 (2008).
[9] M. Geller, F. Hopfer, and D. Bimberg, Microelectron. J. **39**, 302 (2008).
[10] H. Mino, Y. Kouno, K. Oto, K. Muro, R. Akimoto, and S. Takeyama, Appl. Phys. Lett. **92**, 153101 (2008).
[11] S. Kim, Y. T. Lim, E. G. Soltesz, A. M. de Grand, J. Lee, A. Nakayama, J. A. Parker, T. Mihaljevic, R. G. Laurence, D. M. Dor, L. H. Cohn, M. G. Bawendi, and J. V. Frangioni, Nat. Biotechnol. **22**, 93 (2004).
[12] S. W. Hell, Nat. Methods **6**, 24 (2009).
[13] F. Hatami *et al.*, Phys. Rev. B **57**, 4635 (1998).
[14] B. Pal, K. Goto, M. Ikezawa, Y. Masumoto, P. Mohan, J. Motohisa, and T. Fukui, Appl. Phys. Lett. **93**, 073105 (2008).
[15] P. T. K. Chin, C. de Mello Donegá, S. S. van Bavel, S. C. J. Meskers, N. A. J. M. Sommerdijk, and R. A. J. Janssen, J. Am. Chem. Soc. **129**, 14880 (2007).
[16] M. Jones, S. Kumar, S. S. Lo, and G. D. Scholes, J. Phys. Chem. C **112**, 5423 (2008).
[17] A. Fiore, R. Mastria, M. G. Lupo, G. Lanzani, C. Giannini, E. Carlino, G. Morello, M. de Giorgi, Y. Li, R. Cingolani, and L. Manna, J. Am. Chem. Soc. **131**, 2274 (2009).
[18] J. E. Halpert, V. J. Porter, J. P. Zimmer, and M. G. Bawendi, J. Am. Chem. Soc. **128**, 12590 (2006).
[19] D. Oron, M. Kazes, and U. Banin, Phys. Rev. B **75**, 035330 (2007).
[20] W. Zhang, G. Chen, J. Wang, B. Ye, and X. Zhong, Inorg. Chem. **48**, 9723 (2009).
[21] R. Xie, U. Kolb, and T. Basché, Small **2**, 1454 (2006).
[22] A. Pandey and P. Guyot-Sionnest, J. Chem. Phys. **127**, 104710 (2007).
[23] C. de Mello Donegá and R. Koole, J. Phys. Chem. C **113**, 6511 (2009).
[24] S. F. Wuister, C. de Mello Donegá, and A. Meijerink, J. Am. Chem. Soc. **126**, 10397 (2004).
[25] R. Koole, M. M. van Schooneveld, J. Hilhorst, C. de Mello Donegá, D. C. 't Hart, A. van Blaaderen, D. Vanmaekelbergh, and A. Meijerink, Chem. Mater. **20**, 2503 (2008).
[26] C. de Mello Donegá, M. Bode, and A. Meijerink, Phys. Rev. B **74**, 085320 (2006).
[27] P. T. K. Chin, R. A. M. Hikmet, S. C. J. Meskers, and R. A. J. Janssen, Adv. Funct. Mater. **17**, 3829 (2007).
[28] C. de Mello Donegá, S. G. Hickey, S. F. Wuister, D. Vanmaekelbergh, and A. Meijerink, J. Phys. Chem. B **107**, 489 (2003).
[29] R. E. Bailey and S. Nie, J. Am. Chem. Soc. **125**, 7100 (2003).
[30] S. F. Wuister, C. de Mello Donegá, and A. Meijerink, J. Phys.

Chem. B **108**, 17393 (2004).
[31] A. Pandey and P. Guyot-Sionnest, Science **322**, 929 (2008).
[32] R. Koole, P. Schapotschnikow, C. de Mello Donegá, T. J. H. Vlugt, and A. Meijerink, ACS Nano **2**, 1703 (2008).
[33] R. Koole, B. Luigjes, M. Tachiya, R. Pool, T. J. H. Vlugt, C. de Mello Donegá, A. Meijerink, and D. Vanmaekelbergh, J. Phys. Chem. C **111**, 11208 (2007).
[34] D. J. Norris and M. G. Bawendi, Phys. Rev. B **53**, 16338 (1996).
[35] A. Shabaev and A. L. Efros, Nano Lett. **4**, 1821 (2004).
[36] W. Wang, S. Banerjee, S. Jia, M. L. Steigerwald, and I. P. Herman, Chem. Mater. **19**, 2573 (2007).
[37] S. L. Cumberland, K. M. Hanif, A. Javier, G. A. Khitrov, G. F. Strouse, S. M. Woessner, and C. S. Yun, Chem. Mater. **14**, 1576 (2002).
[38] B. S. Santos, G. A. L. Pereira, D. V. Petrov, and C. de Mello Donegá, Opt. Commun. **178**, 187 (2000).
[39] A. L. Efros and A. V. Rodina, Phys. Rev. B **47**, 10005 (1993).
[40] J. Kim, P. S. Nair, C. Y. Wong, and G. D. Scholes, Nano Lett. **7**, 3884 (2007).
[41] B. Henderson and G. F. Imbusch, *Optical Spectroscopy of Inorganic Solids* (Oxford University Press, New York, 1989).
[42] T. J. Liptay, L. F. Marshall, P. S. Rao, R. J. Ram, and M. G. Bawendi, Phys. Rev. B **76**, 155314 (2007).
[43] M. Kuno, J. K. Lee, B. O. Dabbousi, F. V. Mikulec, and M. G. Bawendi, J. Chem. Phys. **106**, 9869 (1997).
[44] A. L. Efros, M. Rosen, M. Kuno, M. Nirmal, D. J. Norris, and M. G. Bawendi, Phys. Rev. B **54**, 4843 (1996).
[45] J. Hu, L. Li, W. Yang, L. Manna, L. Wang, and A. P. Alivisatos, Science **292**, 2060 (2001).
[46] X. Wang, J. Zhang, A. Nazzal, M. Darragh, and M. Xiao, Appl. Phys. Lett. **81**, 4829 (2002).
[47] S. F. Wuister, C. de Mello Donegá, and A. Meijerink, J. Chem. Phys. **121**, 4310 (2004).
[48] B. R. Fisher, H. J. Eisler, N. E. Stott, and M. G. Bawendi, J. Phys. Chem. B **108**, 143 (2004).
[49] Y. Ebenstein, T. Mokari, and U. Banin, Appl. Phys. Lett. **80**, 4033 (2002).
[50] S. F. Wuister, R. Koole, C. de Mello Donegá, and A. Meijerink, J. Phys. Chem. B **109**, 5504 (2005).
[51] A. L. Rogach, T. A. Klar, J. M. Lupton, A. Meijerink, and J. Feldmann, J. Mater. Chem. **19**, 1208 (2009).
[52] A. Narayanaswamy, L. F. Feiner, A. Meijerink, and P. J. van der Zaag, ACS Nano **3**, 2539 (2009).
[53] S. F. Wuister, A. van Houselt, C. de Mello Donegá, D. Vanmaekelbergh, and A. Meijerink, Angew. Chem., Int. Ed. **43**, 3029 (2004).
[54] D. Oron, A. Aharoni, C. de Mello Donegá, J. van Rijssel, A. Meijerink, and U. Banin, Phys. Rev. Lett. **102**, 177402 (2009).
[55] N. Le Thomas, E. Herz, O. Schöps, U. Woggon, and M. V. Artemyev, Phys. Rev. Lett. **94**, 016803 (2005).
[56] J. He, S. S. Lo, J. Kim, and G. D. Scholes, Nano Lett. **8**, 4007 (2008).
[57] H. Wang, C. de Mello Donegá, A. Meijerink, and M. Glasbeek, J. Phys. Chem. B **110**, 733 (2006).
[58] E. Hendry, M. Koeberg, F. Wang, H. Zhang, C. de Mello Donegá, D. Vanmaekelbergh, and M. Bonn, Phys. Rev. Lett. **96**, 057408 (2006).
[59] M. Bayer, P. Hawrylak, K. Hinzer, S. Fafard, M. Korkusinski, Z. R. Wasilewski, O. Stern, and A. Forchel, Science **291**, 451 (2001).
[60] H. J. Krenner, M. Sabathil, E. C. Clark, A. Kress, D. Schuh, M. Bichler, G. Abstreiter, and J. J. Finley, Phys. Rev. Lett. **94**, 057402 (2005).